ELSEVIER

Journal of Structural Geology 29 (2007) 1164–1184

JOURNAL OF STRUCTURAL GEOLOGY

www.elsevier.com/locate/jsg

Cooling induced strain localization in carbonate mylonites within a large-scale shear zone (Glarus thrust, Switzerland)

Andreas Ebert*, Marco Herwegh, Adrian Pfiffner

Institute of Geological Sciences, University of Bern, Baltzerstrasse 1-3, CH-3012 Bern, Switzerland

Received 8 September 2006; received in revised form 19 February 2007; accepted 4 March 2007
Available online 12 March 2007

Abstract

The Glarus thrust (Switzerland) offers a great field example of strain localization under retrograde conditions. Along the thrust, mylonitic microfabrics are characterized by a temperature/stress controlled balance of grain size reducing mechanisms and grain growth. Consequently, mean grain sizes decrease along the thrust with decreasing metamorphic conditions and towards the thrust contact. In an opposite manner, calcite twin densities increase towards the contact. CPOs are strongest between 0.5 and 15 m away from the thrust, but become generally weaker in the last centimeters, where also cataclasites occur. The CPO weakening and grain size reduction towards the shear zone point to a change from predominant dislocation creep to granular flow finally ending in cataclastic deformation. The microfabric changes correlate with a decrease in $\delta^{13}C$ and $\delta^{18}O$ towards the thrust contact indicating the presence of fluids during cycles of brittle and plastic deformation. Based on the microfabric changes, variations in stable isotopes and cross-cut relationships, a subdivision into a low and high-temperature shear zone can be made. The microfabric modifications resulted from changes in deformation conditions due to ongoing thrusting and exhumation induced cooling, promoting further strain localization of an existing high-strain shear zone.

Keywords: Retrograde strain localization; Carbonate mylonites; Microfabric; Glarus thrust; Helvetic Alps

1. Introduction

Large-scale ductile shear zones manifest localization of high shear strains in nature (e.g. Schmid, 1975; Van der Pluijm, 1991; Handy, 1994; Bestmann et al., 2000; Stipp et al., 2002). To localize and keep deformation concentrated in these narrow zones, rock strength has to be weaker than in the surrounding host rock. Such strain softening can be obtained by various processes like dynamic recrystallization, change in deformation mechanisms, synkinematic fluid flow, metamorphic mineral reactions, shear heating, and/or pinning by second-phase particles (e.g. Poirier, 1980; White et al., 1980; Tullis et al., 1982; Hobbs et al., 1990; Olgaard, 1990; Montési and Hirth, 2003; Burlini and Bruhn, 2005). While deformation persists localized during ongoing thrusting, the physical conditions, i.e. the coupled stress–temperature relations can change with time. This was, for example, the case in the Helvetic nappes of the Swiss Alps, where thrusting occurred at peak metamorphism and continued under retrograde conditions (Milnes and Pfiffner, 1980; Groshong et al., 1984; Kirschner et al., 1995, 1996). These exhumation induced changes in extrinsic physical conditions forced the mylonites to adapt their microstructures and CPOs to the new conditions. A typical adaptation to lower temperatures is manifest by grain size reduction (Molli et al., 2000; Herwegh and Pfiffner, 2005; Ebert, 2006) in the shear zone's interior. Simultaneously, the change in microstructure can be accompanied by a decrease in shear zone width (Hull, 1988; Means, 1995). Localization features within sheared rocks were also observed in experiments but mostly strain localized only if a second phase, water or melt was present (Mecklenburgh et al., 1999; Barnhoorn, 2003; Holtzman et al., 2003; Rybacki et al., 2003; Burlini and Bruhn, 2005).

* Corresponding author. Tel.: +41 31 631 8768; fax: +41 31 631 4843.
E-mail address: ebert@geo.unibe.ch (A. Ebert).

0191-8141/$ - see front matter © 2007 Elsevier Ltd. All rights reserved.
doi:10.1016/j.jsg.2007.03.007

Thus, several investigations exist about how strain becomes localized and what factors keep strain localized in a narrow zone. In case of nature, quantitative microfabric analyses, in sections along and perpendicular to the thrust plane, would be required to properly detect strain localization and unravel its evolution in time. Surprisingly, such information is lacking for many prominent large-scale shear zones. In this work, we try to close this gap by a detailed investigation of strain localization in case of the Glarus nappe complex in Switzerland. The following questions will be addressed: How and where do the microfabric and deformation mechanisms change with time within the shear zone? Does the shear zone width change in a systematic way along the thrust? What are the reasons for strain localization and what is the role of fluids and second phases during localization? In the case of the Glarus thrust, for example, variations in stable isotope fractionation across the shear zone as well as the occurrence of synkinematic veins indicate an enhanced fluid flux during formation of the main thrust (Burkhard et al., 1992; Badertscher and Burkhard, 2000; Abart et al., 2002; Abart and Ramseyer, 2002; Badertscher et al., 2002). It is unclear, however, how the change in fluid flux associated isotopic composition is related to microstructural variations with time and what the resulting mechanical consequences for strain localization are.

The Glarus thrust represents an ideal field example, because it is one of the best characterized large-scale thrust zones in the Alps. Metamorphic gradients (e.g. Groshong et al., 1984; Rahn et al., 1995), structural geological features and deformation phases (e.g. Milnes and Pfiffner, 1977, 1980; Groshong et al., 1984; Lihou, 1996), as well as geochemical and isotopic relations (e.g. Burkhard, et al., 1992; Abart et al., 2002; Badertscher et al., 2002) are well established. In this study, carbonates across and along the Glarus thrust were quantitatively analyzed and the observed microstructural variations were correlated with isotopic data of Badertscher (2001). We discuss the change of calcite microfabrics, deformation mechanisms, isotopic composition and their relevance for retrograde strain localization.

2. Analytical methods

To investigate the localization behavior within a large-scale shear zone, samples were collected along the Glarus thrust. The sample localities are labeled, starting with (1) in the north (near Schwanden) and increasing location number towards the south (nr. 8, near Flims, see Fig. 1). They are projected parallel to the temperature isograds in ENE–WSW direction onto the constructed cross section AB that was slightly modified after Pfiffner (1993) and onto the sample profile trace BC (Fig. 1). The profile AB is approximately parallel to the stretching lineation, i.e. parallel to the north-directed thrusting direction. The profile BC used for distance determination between the locations is approximately normal to the peak metamorphic temperature isograds detected in the footwall (see Fig. 1). Resulting distances in between the projected sample locations are around 0.5–8 km (see Fig. 1 and Table 1) corresponding to relative differences in peak metamorphic temperatures of about 5–40 °C between two adjacent locations (see Section 4). To gain insight into the strain localization phenomena, sample profiles perpendicular to the thrust contact were additionally taken at each sample locality in the footwall. In these profiles, rock specimens were collected every centimeter to decimeter in the close vicinity of the thrust contact while the sample distance was increased at distances >1 m from the thrust contact. Locality 2 represents an exception because here, carbonates are also exposed in the hanging wall.

Microstructural analyses were carried out in the *X*-*Z*-plane, where *X* is the stretching lineation and *Z* the axes perpendicular to the foliation. To visualize the grain boundaries and second phases, the surfaces of polished rock chips were etched after Herwegh (2000). From these surfaces, digital SEM images were taken with a Cam Scan (CS4) scanning electron microscope (SEM) equipped with a Noran Voyager 4 image acquisition system. With Adobe Photoshop, the grain boundaries of all phases were manually traced and analyzed by the image analysis software Image SXM (www.liv.ac.uk/~sdb/ImageSXM). From the analyzed grain area, shape (long, short axis), and orientation of calcite, the mean grain size, its distribution, the grain aspect ratio (b/a), and the shape preferred orientation (SPO) were determined. Typically 300–800 calcite grains were analyzed. The resulting mean grain sizes of calcite (D_{cc}) are given as area-weighted values. In this way, the frequency of the grain area distribution has been used to determine the mean grain size represented by the equivalent circular diameter. The calculation and advantage of using area-weighted mean grain sizes is discussed in Ebert (2006) and references therein. Furthermore, the twin density (number of twins per area) was quantitatively determined from the SEM images. Depending of the twin density, 30-600 twin boundaries were counted per sample image. Besides calcite, second-phase particles like sheet silicates, quartz or dolomite were analyzed. To detect and unravel potential influences of second phases on the calcite grain boundaries (pinning), the Zener parameter $Z = d_p/f_p$ was used (Zener in Smith, 1948; Evans et al., 2001; Herwegh and Berger, 2004; Berger and Herwegh, 2004; Ebert, 2006). Z is a geometric factor, determined by the number-weighted mean grain size of second phases (d_p) divided by their volume fraction (f_p). This parameter allows the discrimination between recrystallization and second-phase controlled microfabrics as a function of changes in second-phase size and volume fraction (e.g. Herwegh et al., 2005a).

Textural information of calcite were obtained from EBSD (electron backscatter diffraction, e.g. Venables and Harland, 1973; Adams et al., 1993; and Prior et al., 1996) with a Cam Scan (CS4) scanning electron microscope combined with the Orientation Imaging Microscopy (OIM) data acquisition software from EDAX TSL. An acceleration voltage of 13 kV, a working distance of 17 mm, and a sample tilt of 70° were applied. Depending on the mean grain size, scan step sizes in the range of 5-15 μm were chosen. Stereographic pole figures (2000–40000 orientations) were filtered for confidence indices >0.1. Data contours were calculated by harmonic binning with a maximum expansion of $L = 20$ within the harmonic calculus and a Gaussian smoothing of 10°. The

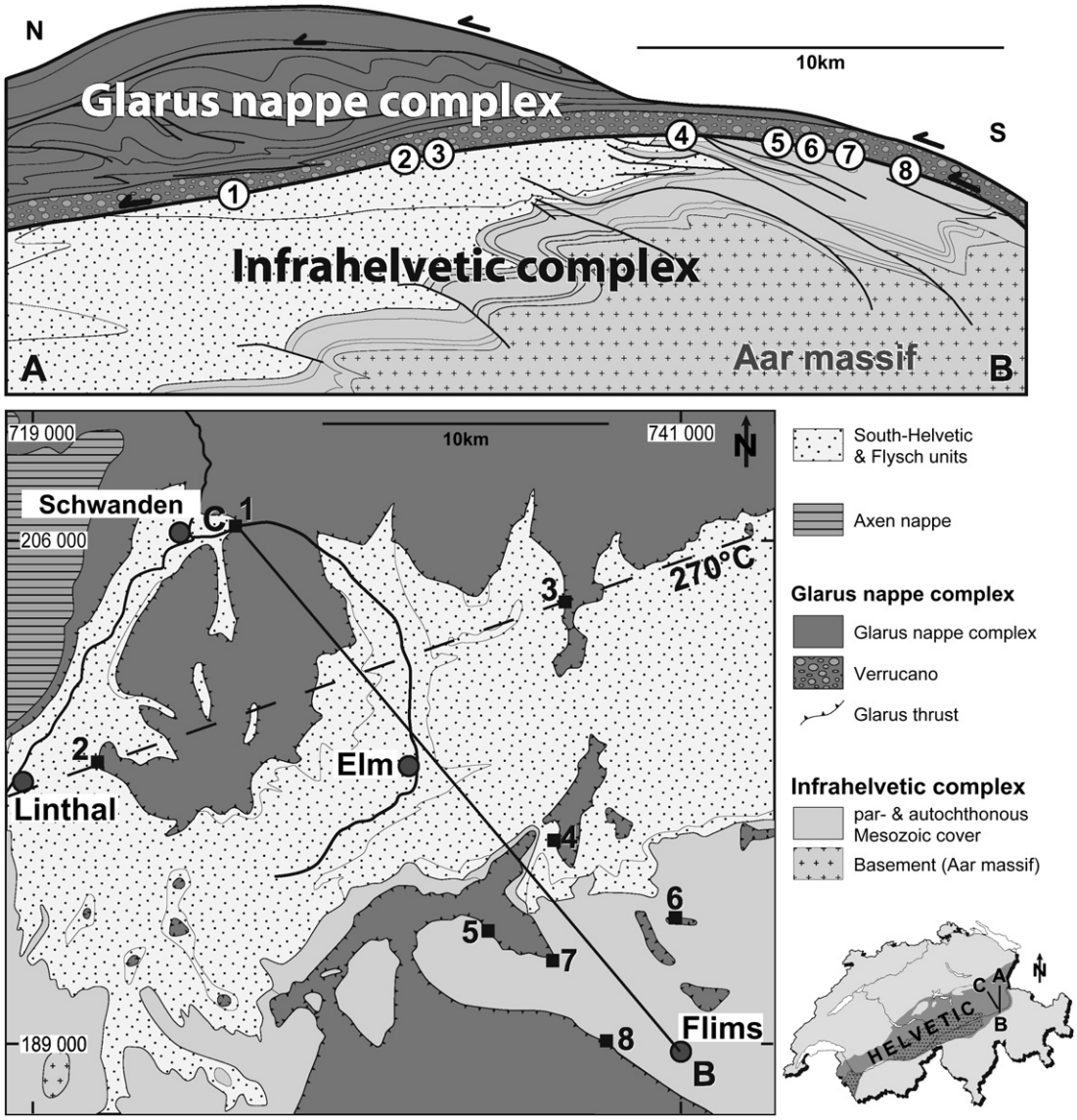

Fig. 1. Cross-section (AB) through the Glarus nappe complex (modified after Pfiffner, 1993) with projected sample locations. Simplified geological map with Swiss coordinates of the studied area (modified after software package: Atlas der Schweiz, 2004) with NW-SE sample profile trace (BC) and the 270 °C-isotherm (dashed line) after Rahn et al. (1995). Numbers represent sample locations starting with (1) at northernmost location (Schwanden) and ending with (8) at southernmost location (Flims).

given texture index J reflects the strength of a CPO (Matthies and Wagner, 1996; Schmocker, 2002). Calcite CPOs were measured for the sample profiles perpendicular to the shear plane for five of the investigated locations.

To improve the temperature gradients in the footwall (Infrahelvtic) in southern parts, we performed calcite-dolomite thermometry. Several dolomite-bearing carbonates were collected in the area of locality 7 and were analyzed with an electron probe micro-analyzer (CAMECA SX 50). To avoid Ca–Mg-diffusion in calcite, a spot size of 15 μm, a current of 10 nA, and acquisition times of 60 s were applied to measure Ca, Mg, Mn, Fe, and Sr. The acceleration voltage was 15 kV. Diffusion can be regarded as negligible, because repeated measurements at the same position showed no variations in element concentrations. Temperatures were calculated after Bickle and Powell (1977), Lieberman and Rice (1986) and Covey-Crump and Rutter (1989). Based on these three calibrations a mean temperature was calculated.

3. Geological setting

The Glarus thrust in the eastern Swiss Alps is the major thrust fault associated with formation of a nappe stack that formed during Oligocene to Miocene from the dismembered former passive continental margin of the Alpine Tethys (e.g. Pfiffner, 1993; Schmid et al., 1996; Stampfli et al., 2002). The Glarus thrust exposes over an area of 600 km^2 with a total displacement of 40–50 km (Pfiffner, 1985). Calc tectonites separate the Glarus nappe complex in the hanging wall from the Infrahelvetic complex in the footwall. It is the lithological difference of green or red Verrucano in the hanging wall and dark Flysch and gray carbonates in the footwall, which

Table 1
Location labels, Swiss coordinates, distances of sample locations from reference point Schwanden (location 1), temperatures, and sampled stratigraphic units

Locality	Location name	Location (Swiss coordinates)	Distance along thrust [km]	T [°C] ±10 °C	Stratigraphic unit
1	Schwanden	726.000/206.350	0	230	Calc-mylonite Tertiary Flysch
2	Sasberg	721.550/198.250	6.23	268	Calc-mylonite Mesozoic carbonate
3	Risetenhoren	737.250/204.350	6.55	270	Calc-mylonite
4	Piz Segnas	737.100/196.100	14.79	320	Cataclasite Calc-mylonite
		737.000/195.600			Mesozoic carbonate
5	Crap Ner	734.500/192.820	16.83	332	Calc-mylonite Mesozoic carbonate
6	Cassons	740.180/193.680	18.2	338	Calc-mylonite Mesozoic carbonate
7	Nagens	736.750/191.980	18.59	343	Calc-mylonite Mesozoic carbonate
8	Plaun	738.270/189.320	21.76	363	Mesozoic carbonate

spectacularly visualizes the Glarus thrust as sharp contact (Fig. 1). The today's Infrahelvetic structures formed as a result of several deformation phases. In the first ones (Pizol and Cavistrau phases), highly allochthonous units (Flysch and South-Helvetic units) were emplaced onto the autochthonous cover (mainly Mesozoic carbonates) of the Aar massif in Early Oligocene times (Pfiffner, 1977; Milnes and Pfiffner, 1977, 1980). Subsequently, the Glarus thrust started to evolve and a fold-and-thrust belt formed in Late Oligocene times (Calanda phase). This phase included ductile deformation under peak metamorphism (Pfiffner, 1977; Milnes and Pfiffner, 1977, 1980; Lihou, 1996). Overprinted Calanda phase cleavage in the vicinity of the Glarus thrust (Milnes and Pfiffner, 1977), inverse metamorphic gradients (Frey, 1988; Rahn et al., 1995), an offset of metamorphic boundaries (Groshong et al., 1984; Rahn et al., 1995), as well as mica ages of Miocene age (Hunziker et al., 1986) indicate that thrusting along the Glarus thrust continued after peak metamorphic conditions (Ruchi phase; Milnes and Pfiffner, 1977).

4. Metamorphism

Based on different geothermometers, peak temperatures of the footwall were determined. Own new data from calcite-dolomite thermometry in the south and temperatures available from literature were compiled to estimate the peak metamorphic conditions at each sample location of this study. Our estimates in the region of localities 5 and 7 yield temperatures in the range of 325–364 °C with an error of ±25 °C (Table 2, Fig. 2). Intense cycles of dynamic recrystallization enhance Ca–Mg exchange between calcite and dolomite allowing temperature estimations by calcite-dolomite thermometry down to 300 °C (Matthews et al., 1999; Bestmann et al., 2000; Herwegh and Pfiffner, 2005; Ebert, 2006). For that reason, Mg/Ca equilibrium between calcite and dolomite can be expected for the recrystallized samples of this study. This is confirmed by the fact that independent of the distance between calcite and dolomite grains, Mg/Ca ratios are similar in the calcite population within a sample. Isotopic quartz–chlorite temperatures (325 ± 30 °C) of Burkhard et al. (1992) from the same location confirm our estimations. Besides these data, further temperature estimates for the rear of the Glarus nappe complex exist, which are based on vitrinite reflectance, chloritoid-chlorite and calcite-dolomite thermometry, and isotopic temperatures (Groshong et al., 1984; Burkhard and Kerrich, 1988; Burkhard et al., 1992; Rahn et al., 2002). They range around 350 °C (Fig. 2). For northern and central parts of this study the detailed temperature determinations of Rahn et al. (1995) were used. They compared a variety of data that are based on mineral parageneses, illite crystallinity, vitrinite reflectance, and fluid inclusions suggesting an increase in metamorphic temperatures from around 230 °C at locality 1 to 300 °C between locality 3 and 4 (Fig. 2). This is in agreement with former studies (e.g. Frey et al., 1980;

Table 2
Locations in Swiss coordinates, temperatures and mean wt% of calcite chemistry ($SrCO_3$ and $MnCO_3$ below detection limit) of samples used for calcite-dolomite thermometry

Location (Swiss coordinates)	T [°C]	$CaCO_3$	$MgCO_3$	$FeCO_3$
736.750/193.020	352 ± 19	0.886 ± 0.003	0.014 ± 0.003	0 ± 0.0003
736.600/192.800	338 ± 10	0.987 ± 0.0004	0.013 ± 0.0004	0
736.080/193.400	325 ± 23	0.823 ± 0.002	0.100 ± 0.002	0
734.950/191.530	364 ± 53	0.869 ± 0.004	0.012 ± 0.008	0.008 ± 0.004
736.550/192.400	333 ± 31	0.983 ± 0.001	0.010 ± 0.001	0.007 ± 0.001

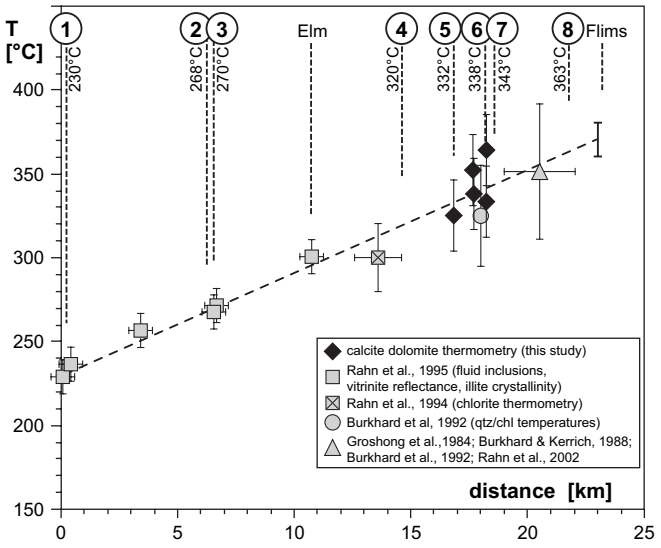

Fig. 2. Estimates of peak metamorphic temperatures along the sample profile BC from N (locality 1) to S (locality 8). Used thermometers and references are given in the legend.

Groshong et al., 1984; Frey, 1988). Temperatures of 300 ± 20 °C from chlorite thermometry were proposed by Rahn et al. (1994) for central parts of our studied section. All these temperature determinations were projected parallel to the isothermes of Rahn et al. (1995) onto our sample profile BC (Fig. 1). A least square regression was calculated to obtain temperatures for each sample location of this study (Fig. 2). Note that the derived temperatures are only valid for the footwall, i.e. the Infrahelvtic units, because due to transported metamorphism, temperatures are higher in the hanging wall. Post-peak metamorphic thrusting offsets the metamorphic boundaries by up to 10 km (Groshong et al., 1984; Frey, 1988; Rahn et al., 1995).

5. Outcrop description

Fig. 3 summarizes the deformation structures in the three main lithological units in the studied area, the Verrucano in the hanging wall, the Infrahelvetic complex in the footwall and the sandwiched tectonites of the Glarus thrust. In the following, the large- to meso-scale deformation structures of these three units will be described in relation to the main deformation phases.

The Permian Verrucano persists mainly of reddish or greenish metamorphosed conglomerates, siltstones, shales, and rare intercalated volcanoclastic horizons. It is characterized by a strong shear plane parallel foliation with increasing mylonitic overprint towards the thrust (e.g. Siddans, 1979; Jagoutz, 2000). N–S stretching lineation as well as extensional crenulation cleavage and asymmetric strain shadows indicate deformation at the base of the Verrucano during the main thrusting of the Glarus nappe complex (Ruchi phase, see e.g. Pfiffner, 1977; Burkhard et al., 1992, and Fig. 3). Despite this deformation, the Verrucano body as entire complex acted as a rigid lid. In contrast to the Infrahelvetic units, large-scale structures like internal thrusts and folds are rare to absent in the Verrucano body (Fig. 1). Note that it is this strength contrast between hanging and footwall, which forced high strain to be localized over a long lasting time at the contact, i.e. in the tectonites of the Glarus thrust.

The Infrahelvetic complex consists of Mesozoic carbonate units that were overthrusted by exotic South-Helvetic and Flysch units during the Pizol phase (Milnes and Pfiffner, 1977; Fig. 1). Today, the footwall of the Glarus thrust in the north consists of these exotic units, while in the south allochthonous to autochthonous massive Cretaceous carbonates dominate. During the main deformation phase of the Infrahelvetic complex (Calanda phase; Milnes and Pfiffner, 1977, 1980; Burkhard et al., 1992), early thrusting, imbrication and large-scale folding occurred resulting in a penetrative south dipping foliation with a N–S to NW–SE directed lineation. In a later stage, during further thrusting of the Glarus nappe complex (Ruchi phase), folds were cut off and large-scale slices of footwall carbonates were transported along the Glarus thrust to the north. The protoliths of the resulting tectonites of the Glarus thrust comprise (a) Mesozoic carbonates from the footwall, (b) newly formed synkinematic calcite veins, and (c) Permian clastics (Verrucano) and Tertiary sandstones and shales (Flysch) that were sheared into the thrust plane. In the north, one tectonite is represented by the famous ‘Lochseitenkalk’ (Heim, 1921; Schmid, 1975), a fault rock consisting of dynamically recrystallized veins that typically show chaotic structures and are responsible for the bright color (e.g. see Badertscher and Burkhard, 2000). To the south, the ‘Lochseitenkalk’ becomes gradually replaced by calc-mylonites (Schmid, 1975; Badertscher and Burkhard, 2000). Besides veins, the bright yellowish color of these mylonites results from a fluid induced bleaching of the Mesozoic carbonates and the occurrence of dolomite. On the outcrop scale, it is important to note that at distances of several meters to decimeters beneath the Verrucano contact, the strongly foliated mylonites are overprinted by asymmetric, north-facing folds. Enclosed with the folding, a steep axial planar cleavage developed. Owing to subsequent thrusting and shearing, folds and cleavage are bent into the shear plane with increasing proximity to the Verrucano contact. In the direct vicinity to the Verrucano contact (dm–cm), white to yellowish mylonites can be observed, which are characterized by a thrust parallel foliation. It is important to note that these mylonites locally cut the folded mylonites, thus indicating a younger age. Within the young mylonites, brittle features are evident in form of cataclasites with angular and/or rounded clasts of vein, footwall, or reworked mylonitic material. Besides these cataclasites, various generations of very thin planar horizons cross-cut all internal structures of the calc-mylonite. They are related to late deformation episodes and are referred to as ‘‘septum’’ (Hsü, 1969; Schmid, 1975).

As will be outlined in more detail below, we will refer in the following to the early and late mylonites, respectively as high and low-temperature shear zone (HT- and LT-SZ, Fig. 3). Note that often the transition between both shear zone types is continuous. This is confirmed by a progressive change in microstructures as will be shown below. For more detailed

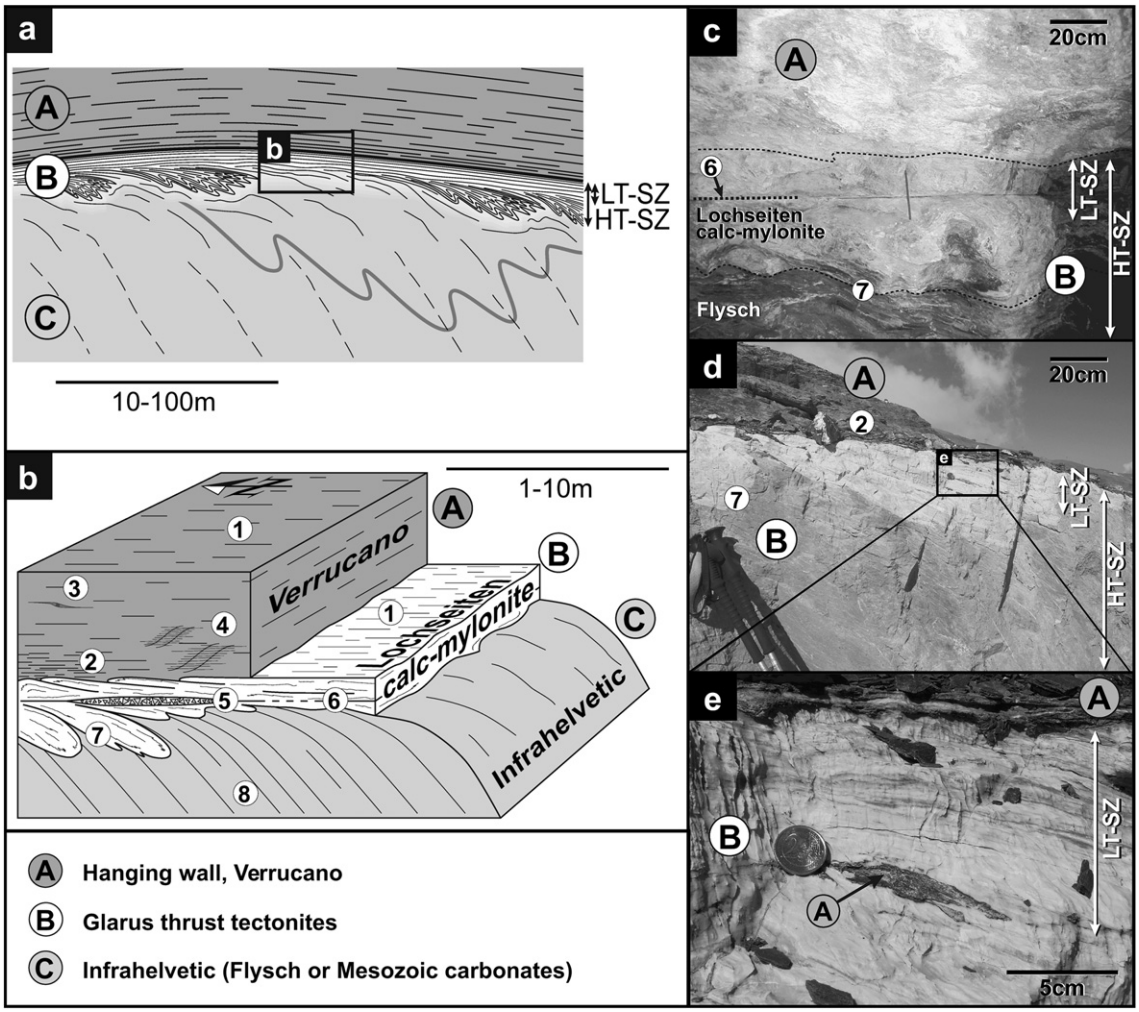

Fig. 3. Deformation structures of the Glarus thrust (A = Verrucano, B = Glarus thrust tectonites, C = Infrahelvetic). (a) Meso- to large-scale structures in the low- (LT-SZ) and high-temperature shear zone (HT-SZ), Verrucano, and Infrahelvetic complex. Inset represents the location of (b). (b) Schematic overview showing deformation structures in the outcrop scale (1) N–S stretching lineation; (2) Ruchi-phase foliation; (3) asymmetric strain fringes; (4) extensional crenulation cleavage; (5) cataclasite; (6) thin sharp mylonitic horizons (''septum''); (7) lobate/cuspate structures; (8) Calanda-phase foliation (modified after Burkhard et al., 1992). (c) Lochseiten calc-mylonite sandwiched between Verrucano and Flysch from location 1; note the sharp layer in the middle represents the septum. View is in direction of stretching lineation. (d) HT-SZ structures affected by later LT-SZ near location 5. Inset represents the location of (e). Sense of shear is top to left (north). (e) Mylonitic fabric of LT-SZ.

macroscopic structural description and interpretation see Schmid (1975), Siddans (1979), Milnes and Pfiffner (1980), Pfiffner, (1977, 1981, 1982), Hirt et al. (1986), Burkhard et al. (1992), Lihou (1996), Badertscher and Burkhard (2000).

6. Quantitative microstructural results

The calcite fabrics in the different carbonate tectonites of the Glarus thrust are characterized by recrystallized grains with different shapes, shape (SPO) and crystallographic (CPO) preferred orientations, and the occurrence of twins (Fig. 4). The intensity of these parameters changes as function of impurity degree, physical conditions and deformation history, i.e. in relation to the distance to the shear plane and from north to south. In the following the variation of the calcite mircofabric is presented.

6.1. Calcite grain size

The mean grain size of recrystallized calcite changes (a) along and (b) with distance to the thrust plane. (a) From north to south the overall grain size increases continuously from 2 to 9 μm in the Lochseiten calc-mylonite at the thrust contact and from >3 to >30 μm in the footwall (Figs. 4, 5 and 6a). Coevally, with increasing metamorphic conditions from north (location 1) to south (locations 7, 8), the widths of grain size distributions widen in the Lochseiten calc-mylonite from 1 to 3 μm, as well as in the deformed footwall from <4 to >10 μm (Fig. 6b). In contrast, the skewness of calcite distributions shows no temperature dependence, but all microstructures reflect distributions, which are symmetric to right skewed (positive skewness, Fig. 6c).

(b) In sections perpendicular to the thrust, the mean grain size decreases stepless towards the thrust contact (Figs. 4, 5 and 6a).

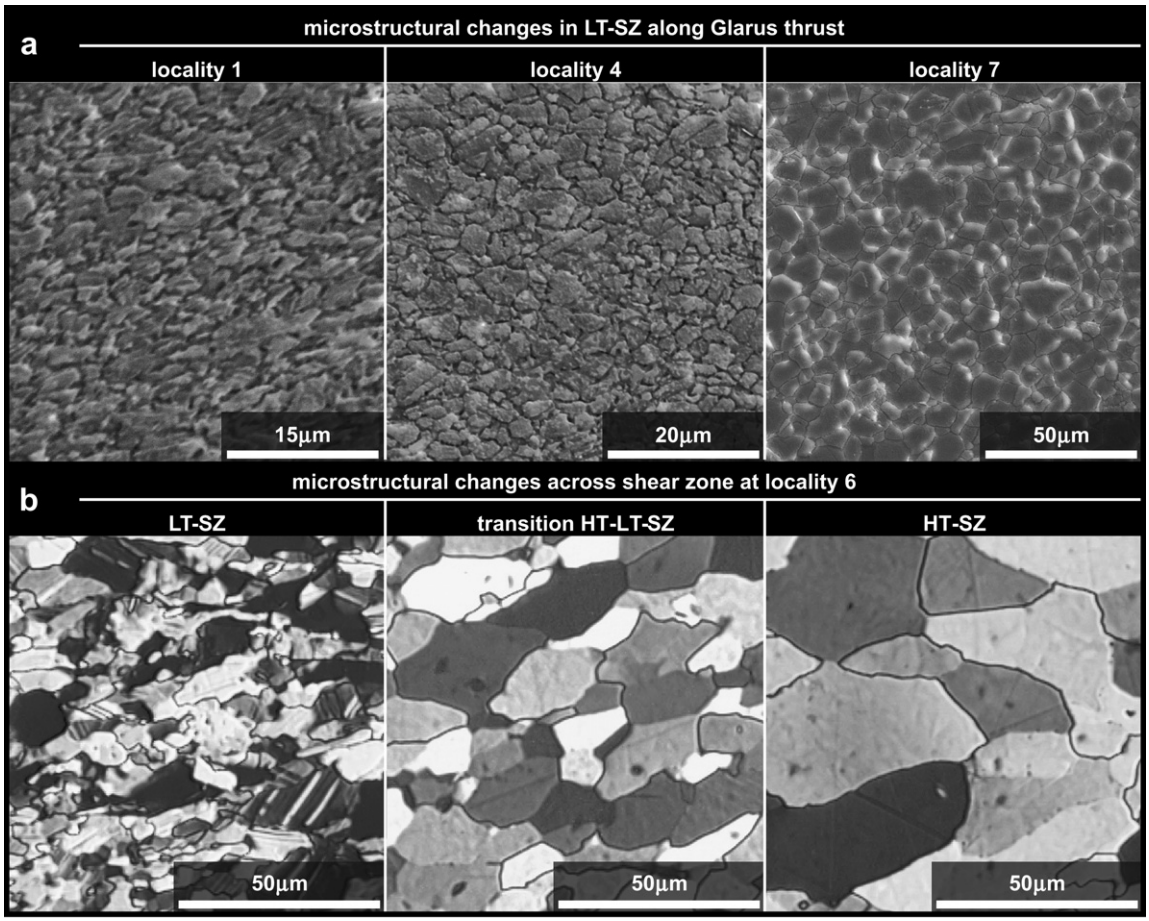

Fig. 4. (a) Microstructural images (first row) are SEM images coming from locations 1, 4, and 7. All belong to the low-temperature shear zone (LT-SZ). (b) Microstructures of thinsections (second row) from the LT- and HT-SZ of location 6. Sense of shear: Top to right (north).

While the change in grain size is only weak in the footwall, a strong decrease in grain size occurs within the last few decimeters beneath the thrust contact (Fig. 5). Total grain size variations across the shear zone are larger in the south (>20 µm) than in the north (<10 µm) (Fig. 6a). These changes of the mean calcite grain size (D_{cc}) in the shear zone in relation to the distance from the thrust plane (d) follow a power-law relation in the form: $D_{cc} = c.d^{0.25}$ with a coefficient c and a constant power exponent reflecting the degree of localization. Outside the HT-SZ, no changes in grain size occur anymore and therefore the power exponent is zero (Figs. 5 and 6). The grain size distribution of calcite behaves similar as the mean grain size showing a decreasing distribution width towards the shear plane (Fig. 6b). The skewness changes only slightly with distance from the shear plane. Near the thrust contact, the distributions are right skewed, while they become more symmetric away from the contact (Fig. 6c).

In some samples within the HT-SZ, small bands (<1 mm) with reduced calcite grain sizes can be observed (Fig. 5, locality 6). Note that the smaller grain size due to the presence of second phases can be excluded since these bands occur in pure calcite layers (see below). This situation therefore might indicate that some parts of the HT-SZ were also affected by the LT deformation.

6.2. Influence of second phases

Carbonates of the footwall and the HT-SZ in southern localities vary in content and type of second phases but generally are quite pure. The observed second phases are dolomite, sheet silicates, quartz, oxides, and/or sulphides. The foliation is manifest by bands of different contents of these phases. In the Lochseiten calc-mylonites, second phases also vary in quantities consisting of dolomite, albite, sheet silicates, and quartz as main minerals. Their content increases from <5 vol% in the footwall carbonate mylonites up to 30 vol% at the thrust contact, while the increase in second phases is most pronounced within the last few centimeter to decimeter. Equiaxed non-deformed grains of dolomite, quartz, and albite are interpreted as secondary syn- to post-tectonically grown phases, where (a) slices of Verrucano were sheared into and mechanically mixed with the calc tectonite and (b) some material infiltrated via fluids loaded with hydration reactions products of the Verrucano (Burkhard et al., 1992; Abart et al., 2002; Hürzeler et al., 2006).

Due to pinning, second phases can retard grain growth resulting in smaller grain sizes in second-phase controlled mylonites compared to the equivalent pure end members (e.g. see Ebert, 2006). To investigate potential effects of second phases, carbonate mylonites with variable contents of second

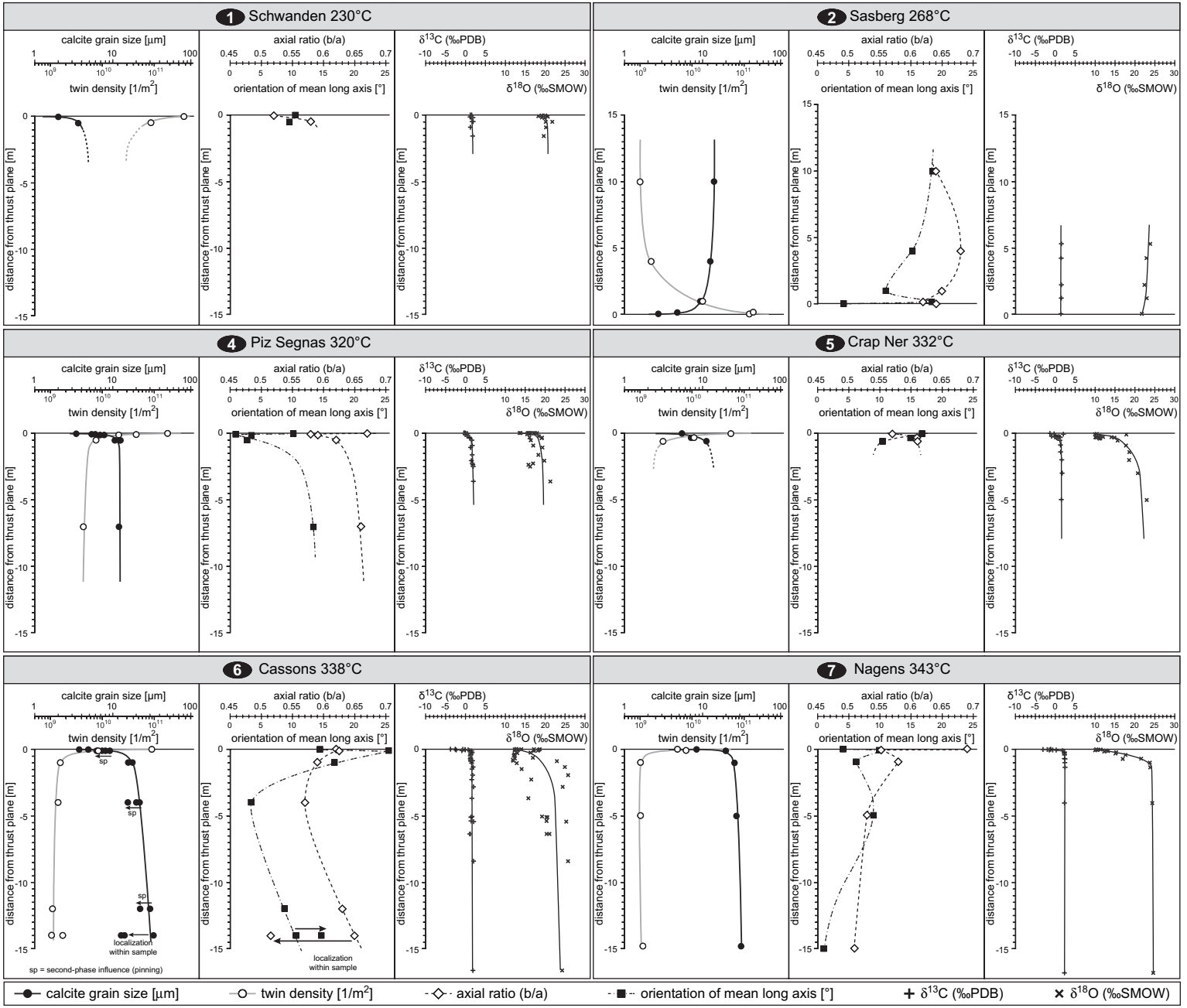

Fig. 5. Change of grain size (black dots), twin density (white dots), axial ratio b/a (white rhombs), and shape preferred orientation SPO (black squares) of calcite in relation of the distance to the thrust contact for sample locations 1, 2, 4–7 (locations 3 and 8 see Figs. 6 and 8). Variations of carbon (+) and oxygen (x) isotopes after Badertscher (2001) for similar locations.

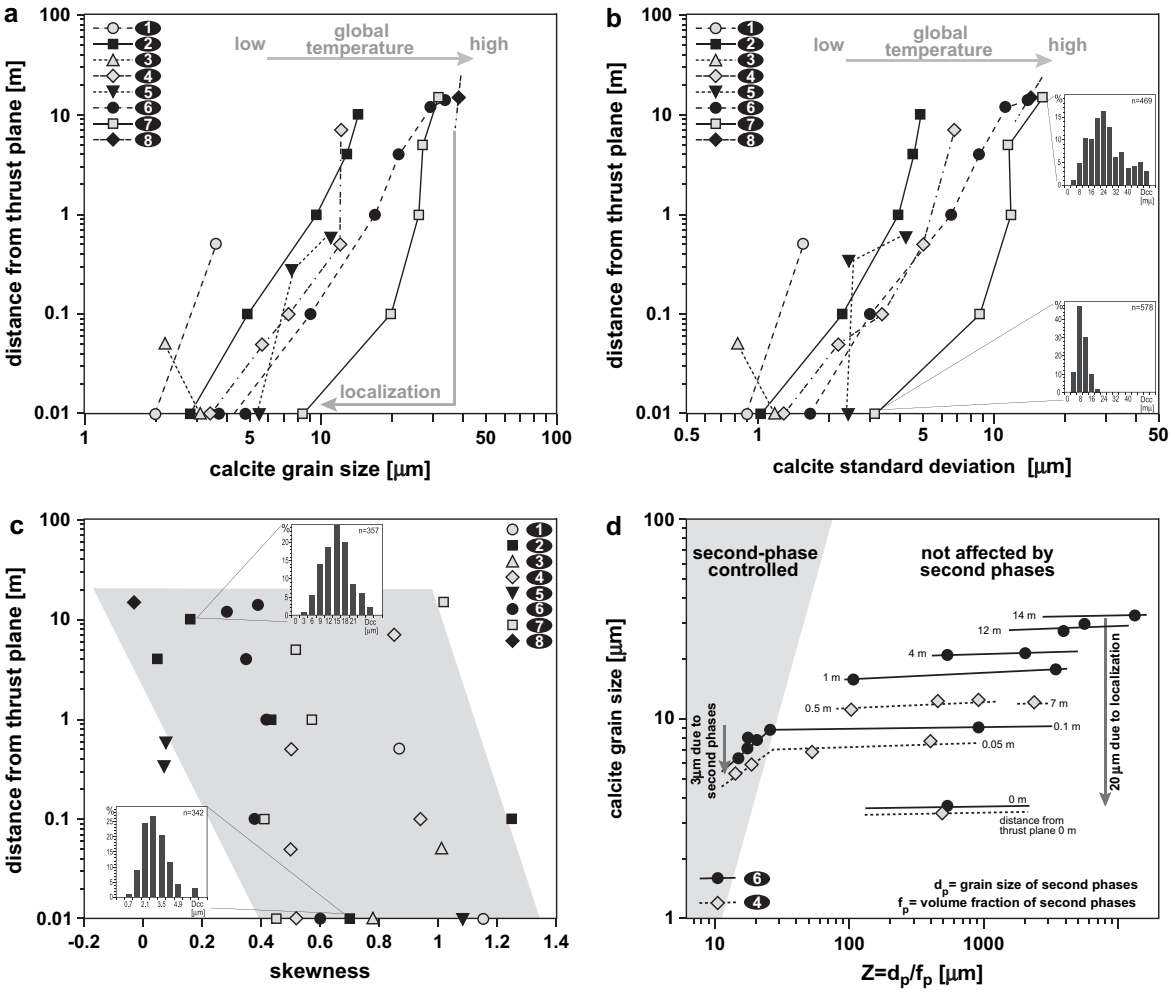

Fig. 6. Change of (a) calcite grain size, (b) width of calcite grain size distribution, (c) skewness of calcite grain size distributions, and (d) second-phase influence (Zener parameter Z) on the calcite grain size in relation to distance from thrust plane for each sample location 1–8.

phases were analyzed for locations 4 and 6. The second-phase influence is expressed by the Zener parameter Z (see Section 2). Fig. 6d illustrates that second-phase particles affected the mean calcite grain size in a similar way as previously observed for other Helvetic nappes (Herwegh et al., 2005a; Ebert, 2006). In the LT-mylonites coming from distances of 5 and 10 cm, respectively, away from the thrust contact, calcite grain sizes are reduced by up to 3 µm in second-phase controlled microstructures (Fig. 6d). Despite this second-phase effect, however, the grain size change across the shear zone in pure samples (high Z values) is much more pronounced (up to 20 µm) than the difference between pure and impure microstructures caused by pinning due to variable contents of second phases. Note that calcite grain sizes are reduced towards the shear zone in both, pure and impure samples, which was already observed for the Morcles nappe (see Ebert, 2006).

6.3. Grain shape and SPO

In the vicinity of the thrust contact, calcite grain boundaries are sutured. However, layers with more equiaxed grains and rather straight grain boundaries are also abundant. In the footwall, the small recrystallized grain fractions show polygonal shapes, while the larger relicts show lobate grain boundaries.

In regard of calcite grain elongation (b/a) and shape preferred orientation (SPO) no clear trends along and across the shear zone can be observed (Fig. 5). Only in the nearest vicinity to the thrust, grains are less elongated, but exceptions occur, e.g. location 1, where grains are more elongated. With respect to location 1, these observations are contrasting previous works of Schmid et al. (1977) and Pfiffner (1982). Furthermore, SPO and grain elongation go hand in hand, except for more spherical grain shapes, where an estimation of grain orientation is not useful since small variations can induce significant data scatter.

6.4. CPO

The crystallographic preferred orientation (CPO) of calcite reflects variations across the shear zone (Fig. 7). Weak to absent CPOs occur in samples at largest distances from the thrust. Towards the thrust contact, at a distance of about 7 m to 50 cm, CPOs tend to be strongest. In the

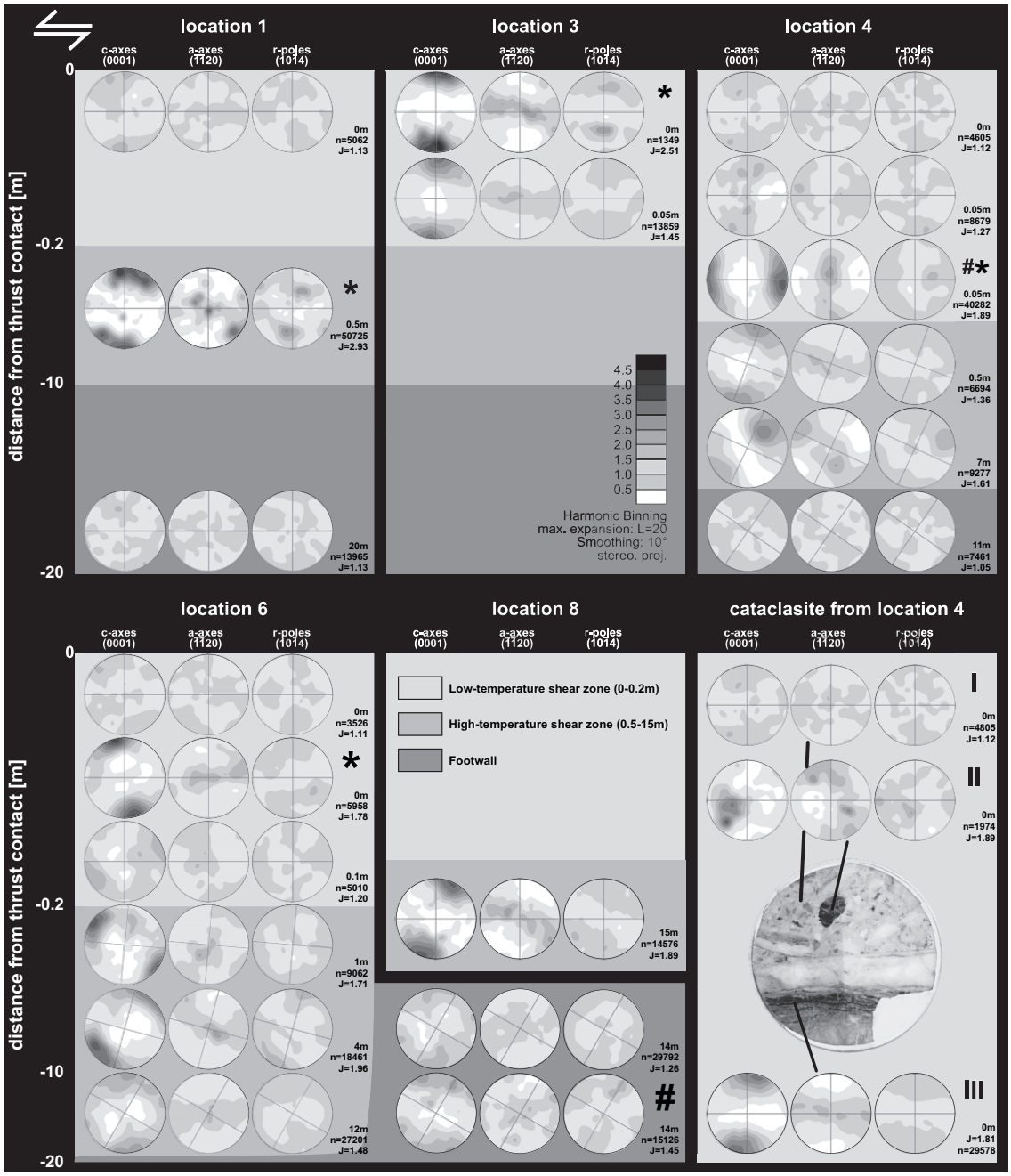

Fig. 7. CPO variations across the shear zone for locations 1, 3, 4, 6, and 8. Light gray, gray, and darker gray backgrounds represent microfabrics from distances between 0–0.1 m, 0.1–10 m, and >10 m from the thrust plane, respectively. The exact distance from the thrust contact, the number of orientations (n), and the texture index (J) are given for each sample analyzed. Pole figures marked by a * indicate CPOs of totally recrystallized very pure vein material in the Lochseiten calc-mylonites. Symbols of # represent thin pure bands with reduced grain sizes, which are explained as small localized shear bands. In case of the tectonic breccia from location 4, the CPO (I) reflects the CPO of the matrix between the clasts with rotated CPOs (II). The cataclasite is situated above a calc-mylonite with very small grain sizes and a strong CPO (III). Pole figures are rotated with respect to the orientation of the foliation in relation to the horizontal thrust plane indicated by the crosses inside each pole figure.

vicinity, i.e. in the last few decimeters to centimeters from the thrust plane, CPO intensities decrease again (see exceptions outlined in Section 6.7). Especially in the HT-SZ, CPOs are rotated in relation to the foliation and thrust plane either anti- or clockwise with respect to shear direction and shear plane.

Besides weak CPOs in the footwall, pure bands with reduced calcite grain sizes show slightly stronger CPOs than the coarser surrounding material (e.g. samples from location 6 at 14 m distance, see Fig. 7, marked with #).

6.5. Twinning

Twinning is abundant in all analyzed calcite microfabrics but the intensity changes along and perpendicular to the shear plane. After Burkhard (1993) and Ferrill et al. (2004) the

dominant twin types in the Mesozoic carbonate mylonites are type II twins, i.e. the twin geometry is characterized by thick and straight twins. Towards the thrust plane, type I twins occur with widths below 1 μm. Despite the high density of the type I twins, type III and IV twins are also marginally abundant. Intersections between different twin types do not indicate that type II to IV necessarily reflect older generations. Rather they coexist with type I twins.

Apart from the change in twin types, the calcite twin density (twins per area) varies and behaves contrary to the calcite grain size change across and along the shear zone. The overall twin density along the thrust increases towards the north from $<10^{10}$ to $>10^{11}$ m^{-2} (Fig. 8). Corresponding to the calcite grain size decrease towards the thrust plane, the twin density increases continuously (Figs. 5 and 8). This change in twin density is found at each sample location, i.e. independent of peak metamorphic conditions.

Semi-quantitative analyses of the mean twin width and mean twin intensity (e.g. Ferrill et al., 2004) reveal values of around 2–10 μm and 7–30 twins per millimeter, respectively, for all samples, except of the LZ-calc-tectonites close to the thrust contact (<50 cm). They display mean twin widths of <1 μm and mean twin intensities of 30–400 per millimeter. Furthermore, the twin width decreases and the twin intensity increases towards northern sample locations.

6.6. Microfabrics of septum and cataclasites

The "septum" and the matrix in cataclasites are characterized by very small calcite grain sizes ranging from <1 μm in fault gauges in the north to 3 μm in southern areas. Note that the septum was not analyzed in this study. For further details see Schmid (1975), Burkhard et al. (1992), and Badertscher and Burkhard (2000).

The clasts of the cataclasites are either angular or rounded and often consist of white and gray limestone clasts with component sizes of up to few centimeters. The investigated cataclasites of this study were not affected by veining during brecciation. The CPO strength measured in components of the tectonic cataclasites also varies in intensity and orientation (Fig. 7, location 4 II). Coarse grained clasts show stronger CPOs than smaller sized ones. The very fine-grained matrix between the clasts is characterized by very weak to absent CPOs (Fig. 7, location 4 I), while mylonitic horizons below this cataclasite represent strong CPOs (Fig. 7, location 4 III), although the calcite grain size is small as well (<5 μm).

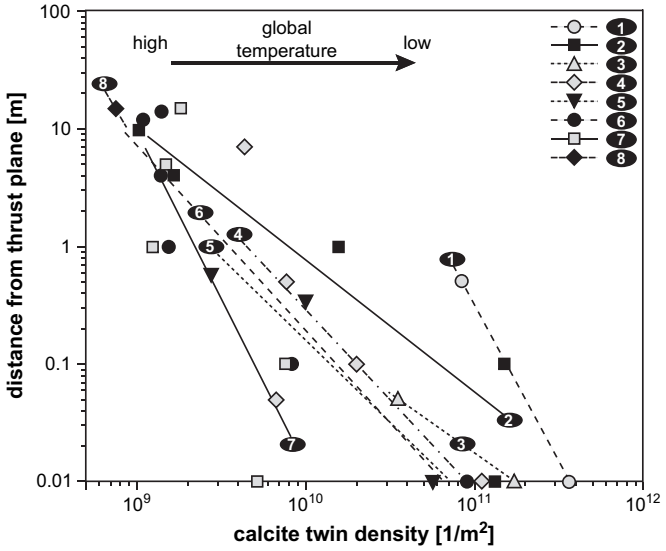

Fig. 8. Continuously increasing twin density (number of twins per area) towards the thrust plane for each sample location 1–8.

6.7. Veining

On the micrometer- to centimeter-scale, bands of fine-grained calcite alternate with calcite veins of different generations, which are often only partly dynamically recrystallized showing large twinned grains. Towards northern locations the alternating thin bands of calcite matrix and veins become more turbulent, i.e. they are intensively folded and sheared. However, veins are also present in the HT-SZ where they often are folded. Dependent on their age of formation, they are not, partly, or totally recrystallized. The latter can be recognized only by relicts that represent few remnants of large twinned calcite grains or by white pure bands with sharp boundaries to the gray host rock. Cathodoluminesence sometimes helped to detect the existence of former veins in completely recrystallized aggregates.

Pure, recrystallized vein material represents an exception in regard of overall weak CPOs in the LT tectonites in the vicinity of the Verrucano contact (location 3, 4, 6, marked with * in Fig. 7). They show strong CPOs with *c*-axis and r-pole maxima. At the same time, surrounding pure and impure calcite microfabrics show only weak CPOs, but note that calcite microstructures (e.g. grain size) are identical in both types.

7. Discussion

As presented above, the Glarus thrust is characterized by (i) rheological contrasts due to the occurrence of different rock types in hanging wall and footwall, (ii) gradients in physical deformation conditions (e.g. temperature) along the thrust, and (iii) continuous changes in these gradients under retrograde metamorphic conditions. All these parameters directly affect the small-scale deformation processes resulting in specific microfabrics and rheology, which in turn control the geometry of the entire shear zone. In the following we will use the microfabrics as key to unravel the effects of (i–iii) in case of the Glarus thrust. For this purpose, we revisit first the concept of dynamic steady state fabrics, which will provide the base for our interpretations ranging from micro- to large-scale.

7.1. The concept of dynamic steady state fabrics

The changes in physical deformation conditions along the Glarus thrust and with time as well as the simultaneous

occurrence of brittle deformation (veining) and mylonitization suggest a rather heterogeneous deformation. Nonetheless, in the area of the active shear zone, deformation was sufficiently strong and homogeneous enough. During each incremental step of strain localization, the host rock, i.e. either pre-existing mylonitic or vein material, adapted its microstructures to the new physical conditions to minimize the total free energy. In this way, dynamically stabilized microfabrics evolved that are characteristic for each specific location along the thrust. They formed by a balance of grain growth and grain size reducing mechanisms (Means, 1981; Herwegh and Handy, 1996; de Bresser et al., 2001). Note that this stabilization is identical to observations from other Helvetic nappes (Herwegh et al., 2005b; Ebert, 2006) and also fits with observations made in experimentally deformed calcite aggregates (Schmid et al., 1987; Rutter, 1995; Pieri et al., 2001; Barnhoorn et al., 2004). Especially synkinematic veins allow the discrimination of a steady state, since they represent markers to compare different stages of ductile deformation ranging from non-, partly, to totally recrystallized vein material. As long as the recrystallized grain size between partly and totally recrystallized vein calcite and host rock is identical, constant deformation conditions can be assumed for the particular strain increment. We used these relationships to identify dynamically stabilized microfabrics for the different stages of deformation along the Glarus thrust. In this context, unimodal Gaussian to slightly right skewed grain size distributions represent additional criteria to detect dynamic steady state.

7.2. Shear zone geometry under high and low temperature conditions

Deformation under retrograde conditions is a common feature in high-strain shear zones, where the width of the shear zone decreases continuously and the microfabric becomes adapted simultaneously to the new conditions with ongoing deformation (e.g. Hull, 1988; Means, 1995; Herwegh and Pfiffner, 2005; Ebert, 2006). A continuation of thrusting during retrograde temperature conditions was also suggested for other Helvetic nappes and seems therefore to represent a common deformation episode during late geodynamic shortening (Herwegh and Pfiffner, 2005; Ebert, 2006). Kirschner et al. (1995, 1996), for example, showed that in the Morcles nappe (western Swiss Alps) ongoing thrusting took place during a retrograde temperature reduction of 30-50 °C. The aforementioned offsets of metamorphic boundaries as well as macro- and microscopic observations along and across the Glarus thrust indicate that a retrograde thrusting also occurred in case of the Glarus nappe complex.

Generally, the shear zone can be divided into a wide high-temperature (HT-SZ) and a narrow low-temperature (LT-SZ) shear zone. The HT-SZ displays ductile deformation fabrics within a zone of up to 2 m in the north and up to 15 m in the south below the thrust contact, which are characterized by mylonitic fabrics, like foliation, plastically deformed veins, and intensive folding on the cm- to m-scale. The microfabrics are characterized by larger dynamic steady state grain sizes, lower twin densities, and generally stronger CPOs than in the LT-SZ (Figs. 5–8). The determination of the shear zone boundary of the HT-SZ is not unambiguous, since the footwall (Infrahelvetic complex) was strained simultaneously, as indicated by finite strains of $R_{xz} = 1.4 - 4$ (Milnes and Pfiffner, 1977; Ring et al., 2001). However, towards the footwall, we define the maximum width of the HT-SZ to be related to the occurrence of the largest recrystallized grain size and the onset of CPO weakening with increasing distance from the thrust contact (Figs. 5–8).

In contrast, the LT-SZ occurs at distances in the decimeter-range below the Verrucano contact and is therefore much smaller than the HT-SZ. The characteristic deformation structures of the LT-SZ overprint the older HT-SZ fabrics. The gradual transition from the HT- to the LT-SZ is marked by a drastic decrease in grain size, a significant increase in twin density, and a transition in CPO strength from strong to rather weak CPOs (Figs. 5–8). Macro- to meso-scale indications from this overprint are fold-like cuspate-lobate structures and the foliation that rotates into the shear zone, as well as increasing brittle features (cataclasites and septums) within the last few decimeters beneath the thrust contact. Folding and shearing of an older mylonitic foliation and an abrupt dissection of this foliation at some locations indicate an overprint of the HT-SZ by the LT-SZ. The latter point would argue for two episodes of thrusting at high- and low-temperature conditions. However, since the offset between HT- and LT-SZ is not evident at each location and a clear transition in micro- as well in meso-scale structures occurs, a continuous decrease in shear zone width and change in thrust activity towards the Verrucano contact during the whole time of retrograde thrusting is more likely.

Information about the retrograde displacement can be obtained from the vertical sample profile of location 2 (Fig. 9). In contrast to all other samples, the analyzed microstructures of this locality belong to the hanging wall. Since at this location, footwall carbonates are absent, predictions about the expected microfabrics can be obtained by extrapolating the grain size trends from all other locations (Fig. 9). The extrapolation reveals too large grain sizes for the carbonate mylonites in the hanging wall compared to the expected ones in the footwall below. Similar grain size trends across shear zones were observed in case of the Doldenhorn nappe (Herwegh and Pfiffner, 2005). Such grain size offsets can be best explained by a formation and freezing in of the hanging wall microstructures further to the south, where the deformation temperatures were higher. Due to retrograde overthrusting, the hanging wall passively moved further to the north resulting in the nowadays exposed offset in calcite grain sizes and twin densities in sections across the shear zone (Fig. 9). Projecting the maximum grain size and/or twin density from the HT-SZ of the hanging wall southwards to identical values of the general N–S trends of the footwall of Fig. 9, allows to quantify the displacement of the hanging wall microfabrics due to retrograde thrusting. The quantification yields a retrograde displacement of approximately 10 km. This approximate value correlates well with the estimates of transported

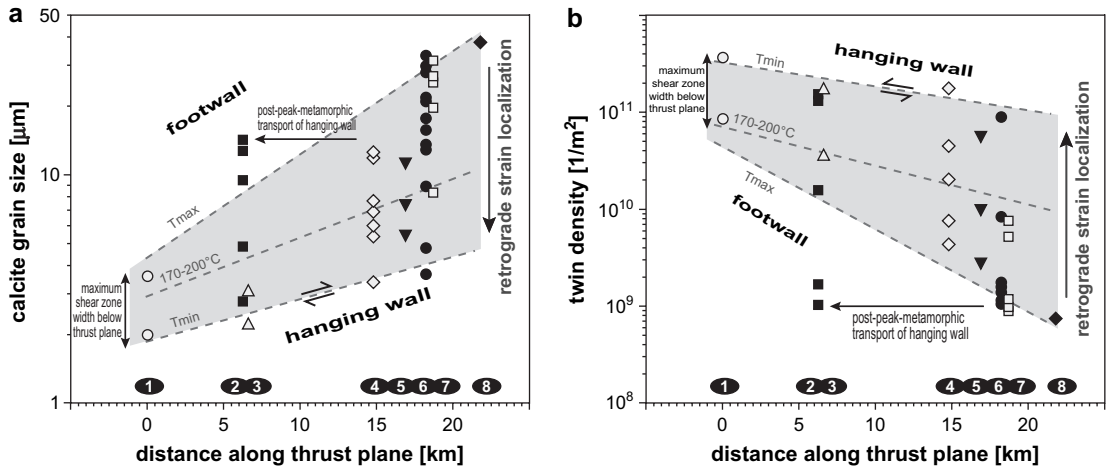

Fig. 9. Relationship between (a) calcite grain size and (b) twin density and distance along and across the shear zone. Maximum grain sizes represent transition between HT-SZ and footwall and allow indirectly the estimation of the maximum shear zone width (see also Fig. 5). Dashed lines reflect temperature conditions and corresponding shear zone width at maximum and minimum temperature conditions, respectively. Line '170–200 °C' was determined from twin intensity–width relations after Ferrill et al. (2004). For further explanations see Section 7.

metamorphism after Groshong et al. (1984), Frey (1988) and Rahn et al. (1995). Assuming a total displacement of the Glarus thrust of 40-50 km, the estimated 10 km of retrograde displacement would indicate 30-40 km of thrusting on the prograde path and particularly during peak metamorphic conditions.

In this context it is important to note that the lateral extension of late brittle structures like cataclasites and faults (septum) are restricted to a few tens of meters. Therefore, the displacement related to these brittle structures could only have accommodated a very small part of the estimated 10 km of retrograde thrusting.

7.3. From HT to LT-SZ: a retrograde change in deformation mechanisms

Over the past decades, different authors observed a variety of different microfabrics in the Glarus overthrust, which led to different interpretations in terms of the mechanisms involved and the resulting mechanical consequences. Weak CPOs, small and equant grains with straight grain boundaries were indicative for Schmid et al. (1977) for superplastic flow. In contrast, some strong CPOs were found by Schmid (1982). This observation, in combination with the occurrence of dynamic recrystallization and fabric internal differences in dislocation densities pointed towards more dislocation creep dominated deformation (Pfiffner, 1982). More recently, Badertscher and Burkhard (2000) suggested episodic activity of brittle faulting and ductile deformation via dislocation creep. Indeed, all deformation structures described by these studies can be found in the Glarus thrust but their focus was mostly restricted to certain parts of the shear zone. As will be demonstrated below, however, the key to solve these apparently contradicting interpretations can be found in a detailed microfabric analysis across the whole shear zone. As discussed in the following, the observed fabrics can be attributed to aforementioned HT and LT structures and therefore display directly the changing deformation mechanisms during retrograde thrusting.

Concave-convex or sutured grain boundaries are typical for grain boundary migration, while the formation of subgrains during grain size reduction of coarse grained vein calcite point to subgrain rotation recrystallization (e.g. Urai et al., 1986). The existence of both recrystallization structures, strong CPOs, large dynamically recrystallized grain sizes, as well as reduced twin densities of calcite point all to dislocation creep as predominant deformation mechanism within the HT-SZ (Figs. 4–7), which would agree with the observations of Pfiffner (1982) for his southern samples. A continuously increasing temperature induced grain growth component towards the south can be interpreted to be responsible for the larger dynamically stabilized calcite grain size in the HT mylonites (Figs. 6 and 9). Recent studies demonstrate that such trends are typical for mid-crustal carbonate shear zones of the Helvetic Alps, where temperature and stress increase and decrease, respectively, towards deeper crustal levels (e.g. Herwegh et al., 2005a,b; Ebert, 2006). Despite this intracrystalline deformation, synkinematic veining indicates activity of brittle faulting and dissolution-precipitation processes. Different generations of recrystallized synkinematic veins point to a cyclical activity of local brittle events during ongoing ductile shearing.

From HT- to LT-SZ microstructures change due to retrograde strain localization. This is manifest by the decrease in grain size, the narrowing of the grain size distribution, the increase in twin density, and the overall weakening in CPOs towards the thrust contact (see Section 6 and Figs. 4–8). Particularly the weak CPOs as well as the very small and equant grain sizes suggest a reduced dislocation creep component and therefore a change in deformation mechanism. For these fabric types, Schmid et al. (1977) and Pfiffner (1982, his northern samples) proposed superplastic flow as

deformation mechanism, where grain boundary sliding was inferred to represent the dominant strain accommodating process. Weakening of the SPO certainly implies an enhanced grain rotation, which in turn has to be accommodated by intergranular processes among which grain boundary sliding is one potential candidate. Also important in this context, however, are mass transfer processes via a fluid incorporating dissolution and precipitation at grain contacts and interfaces. Such mass transfer processes in combination with grain rotation are typical for granular flow as defined by Paterson (1995). The concentrated nucleation of new idiomorphic phases, like dolomite, albite and quartz (see also Hürzeler et al., 2006) in combination with the occurrence of different generations of veins and stylolites support the idea of enhanced mass transport during deformation in close vicinity to the hanging wall contact. Particularly, a dilatational behavior often associated with granular flow (e.g. Paterson, 1995) results in local gradients in permeability, pore pressure and saturation of the fluids allowing local precipitation of new phases. On the other hand, enhanced twinning, local existence of strong CPOs even in the LT-SZ (Fig. 7, see also examples in Schmid, 1982), as well as elongated and sutured dynamically recrystallized grains, still argue for an important share of dislocation creep in the LT-SZ. In this way, deformation in the LT-SZ was not accommodated by a single deformation mechanism but rather displays a complex interaction between granular flow and intracrystalline deformation. A similar combination of deformation mechanisms, i.e. by deformation between the field of power law dislocation creep and superplastic flow, was proposed by Pfiffner (1982) for samples from the south.

The locally observed strong CPOs within the LT-SZ represent outliers (Fig. 7), which occur at each location. Remembering that strong CPOs are always related to completely recrystallized former vein material, the observed CPO intensities might be explained by: (a) differences in finite strain, (b) inheritance of former CPOs, and (c) differences in impurity content. (a) High-strain experiments on calcite show that calcite reaches strong CPOs already at a γ of 5 - 10 (Pieri et al., 2001; Barnhoorn et al., 2004). In terms of shear strains, both HT- and LT-SZ reached much higher shear strains allowing to exclude finite strain as potential reason. (b) Investigations on quartz fibers from the Verrucano of Van Daalen et al. (1999) and retrograde overprinted coarse grained marbles (Bestmann and Prior, 2003) show that there is some control of the host grain CPO on deformation, but with increasing strain and degree of recrystallization the former CPO becomes obliterated. For this reason and because of the fact that the observed non- or partially recrystallized vein material shows no CPO, an inheritance of pre-existing CPOs can be excluded. (c) Impurities like nano- and micro-scale second-phase particles or chemical impurities in calcite can influence the microfabric (e.g. Freund et al., 2001, 2004; Herwegh and Kunze, 2002; Herwegh et al., 2003; Herwegh and Berger, 2004; Ebert, 2006). Particularly pinning/dragging of nano-scale particles (Herwegh and Kunze, 2002) or segregation of chemical impurities in the calcite (Doherty et al., 1997) hinder grain boundary migration reducing the speed of recrystallization cylces (for more detail see Herwegh and Kunze, 2002). In regard of the analyzed CPOs, only samples with limited micro-scale second phase content were investigated. The occurrence of grayish mylonites points to an existence of nano-scale particles (Herwegh and Kunze, 2002). In addition, layers with different cathodoluminescence intensities were observed (similar to Badertscher and Burkhard, 2000) that are caused by variations in trace element contents between vein and grayish material. Hence, nano-scale second phase particles and/or chemical impurities are most likely to be responsible for the observed differences in CPO. In this way, the contributions of dislocation creep and granular flow are higher and lower in white and grayish mylonites, respectively.

Thrust parallel cataclasites and brittle faults (septum) document the final stages of thrusting under brittle conditions. Depending on the local shear strain, pre-existing HT- and LT-fault rocks were overprinted by brittle processes along thin and discrete traces.

7.4. Potential influences of annealing

Elevated temperatures under static conditions might overprint previously evolved deformation microstructures. While such overprints can only weakly modify CPOs, the effect can be more pronounced for grain sizes and grain shapes (e.g. Heilbronner and Tullis, 2002; Barnhoorn et al., 2005; Ebert, 2006). In a critical point of view, therefore, all our inferences related to changes in grain size and shape have to be discussed in terms of static annealing.

Although some samples in the footwall reflect microfabrics with large-sized equant polygonal grains that might indeed be indicative for annealing, the occurrence of elongated grains with SPO, sutured grain boundaries, and subgrains within both HT- and LT-SZ contradict a significant annealing. Furthermore, the distribution is symmetric to slightly right skewed for all analyzed microstructures (Fig. 6c), which is in contrast to Heilbronner and Tullis (2002) and Barnhoorn et al. (2005), where the grain size distribution shifted to larger grain sizes in annealed samples. Last but not least, a significant change of the microstructure under these moderate and decreasing temperature conditions is unlikely as already proposed in Ebert (2006) for samples of the Morcles nappe. In that study, preservation of dislocation structures indicative for deformation, as well as variations in dislocation densities between individual grains contradict a static recovery under such low temperature conditions. This is mainly due to the very low grain boundary mobilities of calcite under static conditions at temperatures lower than 300 °C (for more details see Berger and Herwegh, 2004).

With respect to the observed elongated grain shapes and SPOs, no systematic changes occur across and along the shear zone (Fig. 5), while this is the case for all other microfabric parameters (e.g. grain size and CPO). This fact might imply that grain elongation and SPO manifest the youngest ductile deformation, which was insufficient to adapt grain size and CPO and was not affected by annealing. In this context, experimental observations support the high sensitivity of SPO to

small changes in physical deformation conditions (e.g. Barnhoorn et al., 2004).

7.5. Fluid assisted strain localization

Especially during the stages of ductile deformation as mentioned above, fluids must have been present all the time as indicated by the presence of different generations of synkinematic veins. Therefore, the role of fluids and the related influences on isotopic signatures, microstructures and deformation mechanisms are addressed in this context.

During thrust related deformation, the occurrence of fluids is common in most thrust zones of the Helvetic Alps (e.g. Burkhard et al., 1992; Crespo-Blanc et al., 1995; Kirschner et al., 1999; Badertscher et al., 2002). The interplay between deformation and fluid can lead to strain weakening resulting in strain localization and enhanced fluid flux (e.g. McCaig, 1984, 1989; Oliver, 1986; Carter et al, 1990; Kennedy and Logan, 1997) for the following reasons: (a) permeability contrast, (b) hydrofracturing, (c) smaller grain sizes, and (d) enhanced mass transfer. (a) Due to overthrusting, the Verrucano in the hanging wall with sheet-silicate-rich layers and a thrust parallel foliation acts as a boundary for vertical fluid flux and therefore induces a permeability contrast (Badertscher and Burkhard, 2000; Badertscher et al., 2002). (b) This in turn locally increases pore fluid pressures in the shear zone and can lead to cyclical micro-cracking and fracturing (Hubbert and Rubey, 1959; Jolly and Sanderson, 1997; Badertscher and Burkhard, 2000), which again enhances the permeability and therefore also the channeling effect of fluids along the thrust plane (Marquer and Burkhard, 1992; Badertscher et al., 2002). (c) Latter one is additionally increased by recrystallization induced smaller grain sizes in the shear zone resulting in a larger volume of pathways along calcite grain boundaries. (d) A higher fluid flux enhances pressure solution processes, as evident in form of veins and stylolites, as well as transport of material, and granular flow enabling a faster change in microstructures. All points are given in case of the Glarus thrust. The occurrence of intense synkinematic veining and changes in isotopic signatures of the carbonate mylonites indicate that fluids were present during deformation of both the HT- and LT-SZ. Veins of different generations, i.e. deformed, folded, and recrystallized as well as young undeformed veins cross-cutting older structures characterize all mylonites of the Glarus thrust. The high fluid activity along the Glarus thrust stimulated a number of detailed stable isotopic studies in the footwall, Lochseiten limestone, and Verrucano (Burkhard et al., 1992; Marquer and Burkhard, 1992; Abart et al., 2002; Abart and Ramseyer, 2002; Badertscher et al., 2002).

Fig. 10 compares the $\delta^{13}C$ and $\delta^{18}O$ values from Badertscher (2001) with our interpolated mean calcite grain sizes from Fig. 6a. Both datasets were derived from the same locations (Fig. 1). At a first glance, Fig. 5 indicates that the isotopic composition of calcite goes hand in hand with the change of grain size towards the thrust plane for locations in the south (locations 4–7). However, there exist general differences in changes of isotopic compositions (i) between northern and southern sample locations, (ii) across the shear zone, and (iii) between $\delta^{13}C$, $\delta^{18}O$ trends.

(i) The fact that the stable isotope profiles across the shear zone in the north differ from those in the south (Fig. 5, compare for example locations 1 and 7) was interpreted by Burkhard et al. (1992), Abart et al. (2002), and Badertscher et al. (2002) to be attributed to completely different fluid regimes. The isotopic profile in the north is explained by a strong upward directed flow of fluids that derived from Flysch in the footwall. The impact of this fluid flow was so strong that an isotopic imprint of flow along the thrust was diminished, although the latter one was two to three orders of magnitude higher (Abart et al., 2002). In contrast, in the south, where the footwall consists of Mesozoic limestones, fluids derived from the basement. These fluids migrated along the thrust plane towards the north and were strongly channeled in the thrust (Burkhard et al., 1992; Badertscher et al., 2002).

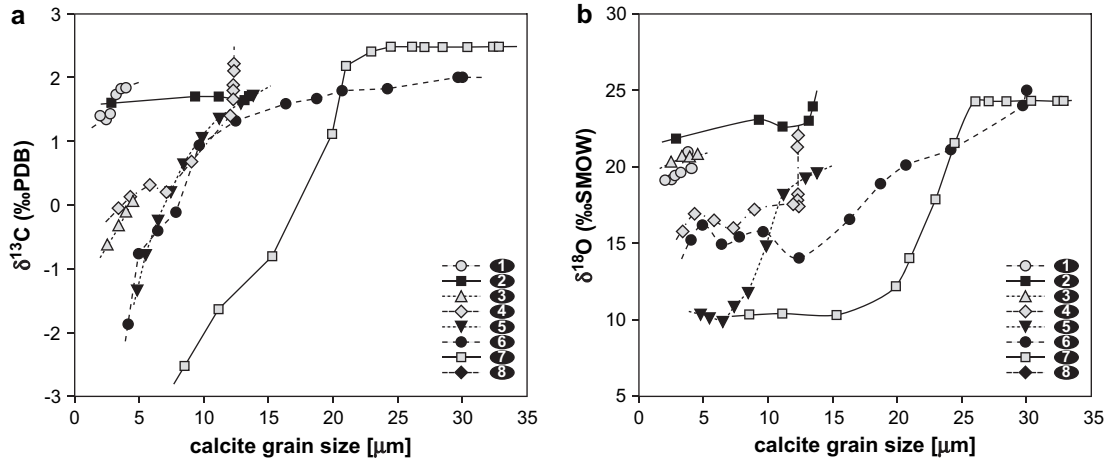

Fig. 10. Relationship between calcite grain size and (a) $\delta^{13}C$ and (b) $\delta^{18}O$ stable isotopes from Badertscher (2001). The calcite grain size reflects indirectly the distance from the thrust plane and was derived from interpolations that are based on Fig. 6a.

(ii) In regard of these southern localities, the correlation between isotopic and microstructure gradients across the shear zone is not surprising since isotopic exchange is enhanced by following points: (a) External fluids are accumulated due to the channeling effect of the shear zone caused by the permeability contrast between Verrucano and footwall. This fact is further supported by an enhanced permeability due to smaller grain sizes in the shear zone and hydrofracturing (Hubbert and Rubey, 1959; Sibson, 1986; Cox et al., 1987; Badertscher and Burkhard, 2000). (b) Recrystallization processes, particularly via grain boundary migration, promote isotopic exchange between fluid and rock (Kirschner et al., 1995; Abart and Ramseyer, 2002; Nakamura et al., 2005). (c) Dissolution, mass transfer along grain boundaries, and precipitation further enhance surface exchange (Criss et al., 1987; McConnell, 1995). (d) Smaller grain sizes facilitate mass transfer along grain boundaries and consequently the possibility of isotopic exchange (Kirschner et al., 1995; Abart and Ramseyer, 2002; Nakamura et al., 2005). (e) Last but not least, higher finite shear strains have been accommodated at the thrust contact, which led to a longer time period of fluid-rock interaction. Note that all these points are also valid for the north but there, the isotopic signature is diminished by the strong vertical fluid flow across the thrust. However, all these points cannot explain, why the isotopic composition of $\delta^{13}C$ is stabilized at a constant value of 2‰ PDB at distances >1 m from the thrust contact, while the calcite grain size still changes (Fig. 10, see locations 6, 7). This discrepancy can either be explained by a shallow imprint of fluids only, too short time available for isotopic exchange, or changes of fluid composition during shear zone evolution from the HT to LT-SZ. Undeformed bleaching fronts as well as newly nucleated second phases in the Lochseiten calc-mylonite, whose material comes via fluids from the Verrucano, would rather argue for the latter point.

(iii) Besides differences in isotopic compositions across the shear zone, $\delta^{18}O$ shows different patterns than $\delta^{13}C$ in southern profiles (Fig. 10). The composition of $\delta^{18}O$ within the LT-SZ is constant indicating that isotopic equilibrium was reached faster than for $\delta^{13}C$ and reaches again constant values at distances >5 m from the thrust contact. This discrepancy can be caused either by faster exchange of ^{18}O than of ^{13}C, varying fluid compositions during time, and/or a later overprint by meteoric fluids. At the present stage it is unclear, which of these points is most realistic.

7.6. Mechanical implications for the formation of the HT- and LT-SZ

In terms of rock strengths, the recrystallized grain size was used in the past to directly infer stress states by paleopiezometry, where a decreasing recrystallized grain size inversely correlates with stress (e.g. Twiss, 1977; Schmid et al., 1980; Rutter, 1995). In case of natural calcite mylonites, the paleopiezometric approach is problematic because the aforementioned stabilization of recrystallized grain sizes via grain growth and grain size reducing mechanisms (e.g. de Bresser et al., 2001; Herwegh et al., 2005b) not only depends on stress but also on temperature and strain rate (see also Austin and Evans, 2007). Moreover, the extrapolation of experimentally obtained calcite flow laws, which are based on a single deformation mechanism, bears severe complications (see de Bresser et al., 2002; Renner and Evans, 2002 and references therein). Promising with this respect are composite flow laws, where the competition between different deformation mechanisms is allowed (e.g. Herwegh et al., 2005b). Following this approach, however, is beyond the scope of this manuscript and will be presented elsewhere. For that reason, we will restrict in the following discussion on relative changes in rock strength only.

Strain rate estimates for the Glarus thrust are in the range of 10^{-10} to 10^{-11} s^{-1} (Schmid, 1975; Pfiffner and Ramsay, 1982; Ebert, 2006). The reduction in shear zone width from south to north (Figs. 5 and 9), for both HT- and LT-SZ, implies a variation in strain rate smaller than one order of magnitude along the thrust at a specific deformation increment. However, a distinction of strain rates between HT- and LT-SZ is difficult to obtain due to lacking age constraints. Two potential scenarios can be considered for retrograde thrusting: (a) an increase in strain rate due to reduction in shear zone width assuming constant plate convergence rates and (b) a constant or even reduced strain rate requiring either changes in plate convergence rates or a strain partitioning by activating additional shear zones at different tectonic levels. Given the observed changes in shear zone width, scenario (a) would imply an increase in strain rate by one to two orders of magnitude, while no predictions are yet possible for (b). However, the reduced shear zone width and the change in deformation mechanisms at lower temperatures indicate a deformation-induced work (the product of stress and strain rate, see Austin and Evans, 2007) that is dissipated within a smaller rock volume and finally ends in form of the discrete brittle structures. This continuous concentration of deformation must be related to the exhumation induced change in deformation temperature.

On the outcrop scale, the occurrence of different generations of veins embedded in a mylonitic matrix was interpreted by Badertscher and Burkhard (2000) to reflect alternating periods of ductile and brittle deformation. This interpretation requires continuous brittle structures interconnected along the entire thrust. In our point of view, this cannot be observed. In contrast, veins and brittle fractures are spatially limited, embedded in a mylonitic matrix, and reflect a temporal variation in their activity. We therefore believe that fracturing and plastic deformation occurred simultaneously. In other words, fractures formed at single locations while at the same time mylonitization continued in the rest of the shear zone providing a continuous supply of synkinematic veins during both ductile HT and LT shearing. Such combined brittle and ductile

deformation is not unique in case of the Glarus thrust and is recently found to be rather common in crustal shear zones (e.g. Fusseis et al., 2006).

The fracturing might be caused by local short time events of seismic activity due to hydrofracturing, followed by time periods of aseismic slip. This is also inferred in other thrusts, like the McConnell thrust in Canada (Kennedy and Logan, 1997) as well as in recently active faults (e.g. Friedrich et al., 2003). Besides the periodic repetition of seismic events, earthquakes occur at different localities along a fault with time (McCalpin and Nishenko, 1996), a point that could explain the limited lateral expansion of cataclasites at various locations along the Glarus thrust. Earthquakes that occur periodically in deep crustal levels, where ductile deformation should be predominant, confirm that brittle events are possible under deformation conditions as inferred for the Glarus thrust.

In terms of the evolution of the entire shear zone, Badertscher and Burkhard (2000) proposed that there is no evidence for a continuous evolution from plastic to brittle deformation with time. Although brittle structures like veins and fractures evolved through the entire activity of the Glarus thrust, our new results contradict the statement of Badertscher and Burkhard (2000) because the continuously decreasing grain size, the increasing twinning, and different generations of recrystallized veins towards the thrust (Figs. 6 and 8) argue all for an overall continuous transition from dislocation creep dominated, over granular flow dominated, towards a pure brittle deformation (cataclasites). This argumentation is further supported by the overprint and local cross-cutting of the HT-structures by the younger LT-SZ. After Ferrill et al. (2004) the decrease in twin width and the increase in twin intensity towards the thrust plane (Fig. 9), simultaneously with the rising twin density (Fig. 8) support a decrease of temperature with time from $>200\,^{\circ}C$ to $<170\,^{\circ}C$ and therefore a change from ductile to brittle deformation conditions. These temperature conditions are confirmed by several points: type I and II twins after Burkhard (1993), which appear under conditions of 150-300 °C, cataclasites, gouge material, and septum-like structures.

In a large-scale point of view the question about the cause of initial strain concentration along the HT-SZ and the subsequent continuous localization of strain into the LT-SZ arises. Different strain softening mechanisms could be listed with this respect, as recently discussed by Burlini and Bruhn (2005). (i) Partial melting and metamorphic mineral reactions (e.g. Mazzucato and Gualtieri, 2000; Cultrone et al., 2001), for example, can be excluded because of temperatures too low for both processes in case of the Glarus thrust. (ii) Second phases as another possibility to reduce the grain size by pinning and therefore acting as a softening parameter (also suggested by Olgaard, 1990) can only be of minor importance in case of the Glarus thrust because both pure as well as impure layers were affected in an identical way by localization. (iii) Shear heating reflects another potential candidate for strain weakening, but would require a temperature rise of few hundred degrees in large-scale shear zones as suggested by Brun and Cobbold (1980). Hence, a grain growth induced larger grain size should be expected in the active shear zone compared to the colder rock fabrics in the hanging and footwall, which is not the case. Moreover, shear heating of several tens to hundred degrees should be detectable with geothermometers, but until now, no temperature increase within the shear zone is indicated. Besides these facts, it is questionable, if under conditions of this study shear heating occurred, because no experimental evidences for shear heating in the ductile field exist so far (Burlini and Bruhn, 2005). (iv) Especially in terms of the early formation of the shear zone, pre-existing mechanical anisotropies have to be considered. In case of Helvetic nappes, inherited zones of weakness like synsedimentary normal faults that were formed at the passive continental margin of the Alpine Tethys (Stampfli et al., 2002; Hänni and Pfiffner, 2001) and the spatial distribution of rock types with different rheology acted as initial weak zones, which determined the nappe stacking in the Helvetic Alps (e.g. Wissing and Pfiffner, 2003). For the Glarus thrust, the sequence of Flysch, carbonates and Verrucano provided strong rheological contrasts, which persisted over the entire history of thrusting. We believe that the overall stress field forced strain to localize preferentially within the carbonates at their contact to the Verrucano due to these anomalies. However, this contrast alone cannot explain the further strain localization during cooling, which might be found in energetic considerations. (v) The total energy input in a deforming volume is based on the applied overall stress field and temperature. At peak metamorphic conditions, the total energy input allowed deformation in the Glarus thrust in a large shear zone volume mainly by dislocation creep. If temperature decreases within a constant overall stress field, the total energy input available for deformation is reduced allowing dislocation creep dominated deformation in a smaller rock volume only. As a consequence, the shear zone width must decrease, as observed in the Glarus thrust. With continuously decreasing temperature, the total energy input becomes too low for dislocation creep. Therefore, a gradual change to more granular flow dominated, and finally brittle deformation has to occur, enclosed with a further reduction in shear zone width (e.g. Fig. 9; Herwegh et al., 2005b; Ebert, 2006). It is the described change in microfabric and shear zone width, which allows to postulate this model for the Glarus thrust. (vi) Strain localization in the aforementioned manner, additionally is enhanced by synkinematic fluids due to faster diffusion, dissolution and mass transfer, a reduced friction, and an increased pore pressure resulting in a local and transient decrease in stress. The latter induced hydrofractring and the formation of synkinematic veins. Furthermore, the fluid flux would have accelerated dynamic recrystallization cycles (see also Herwegh and Jenni, 2001; Ebert, 2006). The fact that the cataclasites and septum as youngest brittle structural elements are vein-free and not deformed, suggest an end of fluid flux and thrusting of the Glarus nappe at time of last cataclastic deformation. This in turn reveals that below a critical temperature and break off of fluid flow as important weakening parameter, the shear zone becomes rheologically too strong for further deformation forcing large-scale strain to localize within an other tectonic level in order to be able to accommodate further large-scale compression.

To summarize, strain localization is a continuous process in a large-scale shear zone under retrograde conditions, where the microfabric becomes adapted to the new extrinsic conditions (e.g. reduced temperature) all the time. In turn, the modifications of the rock fabrics are based on changes in the energy available, its work dissipation and the adaptation in deformation mechanisms.

8. Conclusions

On first glance, the observations made in case of the Glarus thrust are similar to conventional strain gradients suggested for many shear zones. There, strain gradients evolve due to ongoing shearing characterized by slightly deformed protoliths at the rim of the shear zone, subsequent increase in mylonitization towards the shear zone center ending in an ultramylonite (Fig. 11 right side, e.g. see also Van der Pluijm, 1991; Busch and Van der Pluijm, 1995; Molli and Heilbronner, 1999; Bestmann et al., 2000). The resulting microfabrics typically show bimodal grain size distributions for the protomylonites, where the sizes of recrystallized grains and subgrains are similar to the grain size in the shear zone center (e.g. Molli and Heilbronner, 1999; Pieri et al, 2001; Bestmann and Prior, 2003). Furthermore, the grain relicts of the protoliths are elongated and intensively twinned, while twinning in the ultramylonite is low. For temperatures similar to those of this study, mainly twins of type III and IV would be expected in these relicts (Burkhard, 1993; Molli and Heilbronner, 1999). Additionally, core-mantel structures occur in the transition zone between protolith and mylonite (Van der Pluijm, 1991; Passchier and Trouw, 1996; Bestmann et al., 2000). The ultramylonite in the shear zone is characterized by steady state microfabrics with an unimodal very small grain size with only slightly elongated grains and strong CPOs (Van der Pluijm, 1991; Busch and Van der Pluijm, 1995; Bestmann et al., 2000). Furthermore, CPO intensities would increase continuously towards the shear zone. However, the Glarus thrust shows distinct differences. The most striking point is a relative difference in age between LT and HT parts of the shear zone, where the latter are folded and locally cut off by the younger ones. Furthermore, the calcite grain size, as well as the width of the distribution decrease continuously towards the thrust plane with an enhanced grain size reduction within the last few decimeters (Figs. 5 and 11). In fact, symmetric to slightly right-sided skewed grain sizes across the whole Glarus thrust indicate that dynamic steady state was reached in each part of the localized shear zone. Simultaneously, the CPO intensity increases towards the shear plane, but within the LT-SZ the overall CPO intensity is reduced again (Figs. 7 and 11). While mainly type I and II twins are abundant, the twin density increases in an opposite manner as the calcite grain size decreases. The latest overprint under coolest metamorphic conditions is evident in form of cataclasites and/or very thin and sharp bands of gouge or very fine-grained calcitic matrix. All these points contradict a simple shear strain gradient, where the structures across the shear zone formed at the same time. Note that retrograde strain localization, however, does not exclude an increase in total strain and strain rate towards the thrust plane. The special situation of the Glarus thrust, involving a displacement as large as 50 km accommodated within a relatively narrow zone over a long lasting deformation history under peak and retrograde metamorphic conditions, is due to the strong rheological contrast between foot- and hanging wall. Such cooling induced localization might be present in other mid-crustal shear zones as well, requiring more detailed studies in this direction.

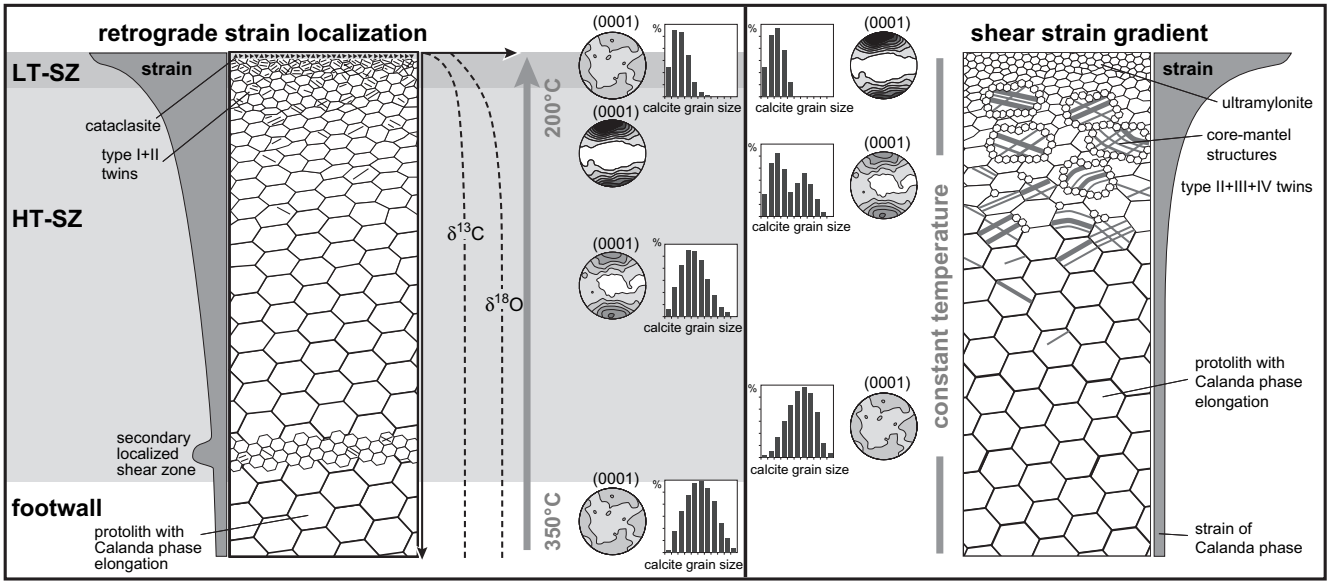

Fig. 11. Schematic changes in microstructure and CPO of calcite in case of a temperature induced strain localization (left side) and as a result of a simple shear strain gradient across the shear zone at constant temperature (right side). Isotopes $\delta^{13}C$ and $\delta^{18}O$, CPOs of calcite c-axes, histograms of mean calcite grain size (area-weighted), and twin types after Burkhard (1993). LT- and HT-SZ = low and high-temperature shear zone. Note that isotopic imprint as well as secondary localized shear zones are also possible in case of the shear strain gradient.

Acknowledgements

The Swiss National Sciences Foundation is gratefully acknowledged, which supported this project by grants 21-66889.01 and 200020-103720. The reviewers L. Kennedy and M. Stipp are thanked for their helpful and detailed reviews and constructive criticism.

References

Abart, R., Ramseyer, K., 2002. Deformation induced quartz-fluid oxygen isotope exchange during low-grade metamorphism: an example from the Glarus thrust, E Switzerland. Schweizerische Mineralogische und Petrographische Mitteilungen 82, 291–302.

Abart, R., Badertscher, N., Burkhard, M., Povoden, E., 2002. Oxygen, carbon and strontium isotope systematics in two profiles across the Glarus thrust: implications for fluid flow. Contributions to Mineralogy and Petrology 143 (2), 192–208.

Adams, B.L., Wright, S.I., Kunze, K., 1993. Orientation imaging: the emergence of a new microscopy. Metallurgical Transactions 24A (4), 819–830.

Atlas der Schweiz, 2004. Software Version 2.0. Swiss Federal Office of Topography (swisstopo), Wabern, Switzerland.

Austin, N.J., Evans, B., 2007. Paleowattmeters: A scaling relation for dynamically recrystallized grain size. Geology 35 (4), 343–346.

Badertscher, N., 2001. Deformation Mechanisms and Fluid Flow Along the Glarus Overthrust, Eastern Helvetic Alps, Switzerland. Ph.D. thesis, Université de Neuchâtel, Switzerland.

Badertscher, N.P., Burkhard, M., 2000. Brittle–ductile deformation in the Glarus thrust Lochseiten (LK) calc-mylonite. Terra Nova 12 (6), 281–288.

Badertscher, N.P., Abart, R., Burkhard, M., McCaig, A., June 2002. Fluid flow pathways along the Glarus overthrust derived from stable and Sr-isotope patterns. American Journal of Science 302, 517–547.

Barnhoorn, A., 2003. Rheological and Microstructural Evolution of Carbonate Rocks During Large Strain Torsion Experiments. Ph.D. thesis, ETH, Zürich, Switzerland.

Barnhoorn, A., Bystricky, M., Burlini, L., Kunze, K., 2004. The role of recrystallisation on the deformation behaviour of calcite rocks: large strain torsion experiments on Carrara marble. Journal of Structural Geology 26 (5), 885–903.

Barnhoorn, A., Bystricky, M., Burlini, L., Kunze, K., 2005. Post-deformational annealing of calcite rocks. Tectonophysics 403 (1–4), 167–191.

Berger, A., Herwegh, M., 2004. Grain coarsening in contact metamorphic carbonates: effects of second-phase particles, fluid flow and thermal perturbations. Journal of Metamorphic Geology 22 (5), 459–474.

Bestmann, M., Prior, D.J., 2003. Intragranular dynamic recrystallization in naturally deformed calcite marble: diffusion accommodated grain boundary sliding as a result of subgrain rotation recrystallization. Journal of Structural Geology 25 (10), 1597–1613.

Bestmann, M., Kunze, K., Matthews, A., 2000. Evolution of a calcite marble shear zone complex on Thassos Island, Greece: microstructural and textural fabrics and their kinematic significance. Journal of Structural Geology 22 (11–12), 1789–1807.

Bickle, M.J., Powell, R., 1977. Calcite-dolomite geothermometry for iron-bearing carbonates. Contributions to Mineralogy and Petrology (Historical Archive) 59 (3), 281–292.

Brun, J.P., Cobbold, P.R., 1980. Strain heating and thermal softening in continental shear zones: a review. Journal of Structural Geology 2 (1–2), 149–158.

Burkhard, M., Kerrich, R., 1988. Fluid regimes in the deformation of the Helvetic nappes, Switzerland, as inferred from stable isotope data. Contributions to Mineralogy and Petrology 99 (4), 416–429.

Burkhard, M., 1993. Calcite twins, their geometry, appearance and significance as stress-strain markers and indicators of tectonic regime: a review. Journal of Structural Geology 15 (3–5), 351–368.

Burkhard, M., Kerrich, R., Maas, R., Fyfe, W.S., 1992. Stable and Sr-isotope evidence for fluid advection during thrusting of the Glarus nappe (Swiss Alps). Contributions to Mineralogy and Petrology 112 (2–3), 293–311.

Burlini, L., Bruhn, D., 2005. High-strain zones: laboratory perspectives on strain softening during ductile deformation. In: Bruhn, D., Burlini, L. (Eds.), High-Strain Zones: Structure and Physical Properties. Geological Society, London, Special Publications, vol. 245, pp. 1–24.

Busch, J.P., Van der Pluijm, B.A., 1995. Calcite textures, microstructures and rheological properties of marble mylonites in the Bancroft shear zone, Ontario, Canada. Journal of Structural Geology 17 (5), 677–688.

Carter, N.L., Kronenberg, A.K., Ross, J.V., Wiltschko, D.V., 1990. Control of fluids on deformation of rocks. In: Knipe, R.J., Rutter, E.H. (Eds.), Deformation Mechanisms, Rheology and Tectonics. Geological Society, London, Special Publications, vol. 54, pp. 1–13.

Covey-Crump, S.J., Rutter, E.H., 1989. Thermally-induced grain growth of calcite marbles on Naxos Island, Greece. Contributions to Mineralogy and Petrology (Historical Archive) 101 (1), 69–86.

Cox, S.F., Etheridge, M.A., Wall, V.J., 1987. The role of fluids in syntectonic mass transport, and the localization of metamorphic vein-type ore deposists. Ore Geology Reviews 2 (1–3), 65–86.

Crespo-Blanc, A., Masson, H., Sharp, Z., Cosca, M., Hunziker, J., 1995. A stable and $^{40}Ar/^{39}Ar$ isotope study of a major thrust in the Helvetic nappes (Swiss Alps): evidence for fluid flow and constraints on nappe kinematics. Geological Society of America Bulletin 107 (10), 1129–1144.

Criss, R.E., Gregory, R.T., Taylor, J.H.P., 1987. Kinetic theory of oxygen isotopic exchange between minerals and water. Geochimica et Cosmochimica Acta 51 (5), 1099–1108.

Cultrone, G., Rodriguez-Navarro, C., Sebastian, E., Cazalla, O., De La Torre, M.J., 2001. Carbonate and silicate phase reactions during ceramic firing. European Journal of Mineralogy 13 (3), 624–634.

de Bresser, J.H.P., Ter Heege, J.H., Spiers, C.J., 2001. Grain size reduction by dynamic recrystallization: can it result in major rheological weakening? International Journal of Earth Sciences 90 (1), 28–45.

de Bresser, J.H.P., Evans, B., Renner, J., 2002. Predicting the strength of calcite rocks under natural conditions, deformation mechanisms, rheology and tectonics: current status and future perspectives. Geological Society of London, Special Publications, pp. 309–329.

Doherty, R.D., Hughes, D.A., Humphreys, F.J., Jonas, J.J., Jensen, D.J., Kassner, M.E., King, W.E., McNelley, T.R., McQueen, H.J., Rollett, A.D., 1997. Current issues in recrystallization: a review. Materials Science and Engineering A 238 (2), 219–274.

Ebert, A., 2006. Microfabric Evolution in Pure and Impure Carbonate Mylonites and Their Role for Strain Localization in Large-scale Shear Zones. Ph.D. thesis, University of Bern, Switzerland.

Evans, B., Renner, J., Hirth, G., 2001. A few remarks on the kinetics of static grain growth in rocks. International Journal of Earth Sciences 90 (1), 88–103.

Ferrill, D.A., Morris, A.P., Evans, M.A., Burkhard, M., Groshong, J., Richard, H., Onasch, C.M., 2004. Calcite twin morphology: a low-temperature deformation geothermometer. Journal of Structural Geology 26 (8), 1521–1529.

Freund, D., Rybacki, E., Dresen, G., 2001. Effect of impurities on grain growth in synthetic calcite aggregates. Physics and Chemistry of Minerals 28 (10), 737–745.

Freund, D., Wang, Z., Rybacki, E., Dresen, G., 2004. High-temperature creep of synthetic calcite aggregates: influence of Mn-content. Earth and Planetary Science Letters 226 (3–4), 433–448.

Frey, M., Teichmüller, M., Teichmüller, R., Mullis, J., Künzli, B., Breitschmid, A., Gruner, U., Schwizer, B., 1980. Very low-grade metamorphism in external parts of the Central Alps: Illite crystallinity, coal rank and fluid inclusion data. Eclogae geologicae Helvetiae 73 (1), 173–203.

Frey, M., 1988. Discontinuous inverse metamorphic zonation, Glarus Alps, Switzerland: evidence from illite crystallinity data. Schweizerische Mineralogische und Petrographische Mitteilungen 68, 171–184.

Friedrich, A.M., Wernicke, B.P., Niemi, N.A., Bennett, R.A., Davis, J.L., 2003. Comparison of geodetic and geologic data from the Wasatch region, Utah, and implications for the spectral character of Earth deformation at periods of 10 to 10 million years. Journal of Geophysical Research 108 (B4), doi:10.1029/2001JB000682.

Fusseis, F., Handy, M.R., Schrank, C., 2006. Networking of shear zones at the brittle-to-viscous transition (Cap de Creus, NE Spain). Journal of Structural Geology 28, 1228–1243.

Groshong, R.H., Pfiffner, O.A., Pringle, L.R., 1984. Strain partitioning in the Helvetic thrust belt of eastern Switzerland from the leading edge to the internal zone. Journal of Structural Geology 6 (1–2), 5–18.

Hänni, R., Pfiffner, O.A., 2001. Evolution and internal structure of the Helvetic nappes in the Bernese Oberland. Eclogae Geologicae Helvetiae 94 (2), 161–171.

Handy, M.R., 1994. The energetics of steady state heterogeneous shear in mylonitic rock. Materials Science and Engineering A 175 (1–2), 261–272.

Heilbronner, R., Tullis, J., 2002. The effect of static annealing on microstructures and crystallographic preferred orientations of quartzites experimentally deformed in axial compression and shear. In: de Meer, S., Martyn, R.D., de Bresser, J.H.P., Gill, M.P. (Eds.), Deformation mechanisms, Rheology and Tectonics. Geological Society, London, Special Publications, vol. 200, pp. 191–218.

Heim, A., 1921. Geologie der Schweiz, Bd 2. Tauchniz, Leipzig.

Herwegh, M., Berger, A., 2004. Deformation mechanisms in second-phase affected microstructures and their energy balance. Journal of Structural Geology 26 (8), 1483–1498.

Herwegh, M., Handy, M.R., 1996. The evolution of high-temperature mylonitic microfabrics: evidence from simple shearing of a quartz analogue (norcamphor). Journal of Structural Geology 18 (5), 689–710.

Herwegh, M., Jenni, A., 2001. Granular flow in polymineralic rocks bearing sheet silicates: new evidence from natural examples. Tectonophysics 332 (3), 309–320.

Herwegh, M., Kunze, K., 2002. The influence of nano-scale second-phase particles on deformation of fine grained calcite mylonites. Journal of Structural Geology 24 (9), 1463–1478.

Herwegh, M., Pfiffner, O.A., 2005. Tectono-metamorphic evolution of a nappe stack: a case study of the Swiss Alps. Tectonophysics 404 (1–2), 55–76.

Herwegh, M., 2000. A new technique to automatically quantify microstructures of fine grained carbonate mylonites: two-step etching combined with SEM imaging and image analysis. Journal of Structural Geology 22 (4), 391–400.

Herwegh, M., Berger, A., Ebert, A., 2005a. Grain coarsening maps: a new tool to predict microfabric evolution of polymineralic rocks. Geology 33 (10), 801–804.

Herwegh, M., de Bresser, J.H.P., ter Heege, J.H., 2005b. Combining natural microstructures with composite flow laws: an improved approach for the extrapolation of lab data to nature. Journal of Structural Geology 27 (3), 503–521.

Herwegh, M., Xiao, X.H., Evans, B., 2003. The effect of dissolved magnesium on diffusion creep in calcite. Earth and Planetary Science Letters 212 (3–4), 457–470.

Hirt, A.M., Lowrie, W., Pfiffner, O.A., 1986. A paleomagnetic study of tectonically deformed red beds of the lower Glarus nappe complex, eastern Switzerland. Tectonics 5 (5), 723–731.

Hobbs, B.E., Mühlhaus, H.B., Ord, A., 1990. Instability, softening and localization of deformation. In: Knipe, R.J., Rutter, E.H. (Eds.), Deformation Mechanisms, Rheology and Tectonics. Geological Society, London, Special Publications, vol. 54, pp. 143–165.

Holtzman, B.K., Kohlstedt, D.L., Zimmerman, M.E., Heidelbach, F., Hiraga, T., Hustoft, J., 2003. Melt segregation and strain partitioning: implications for seismic anisotropy and mantle flow. Science, New Series 301, 1227–1230.

Hsü, K.J., 1969. A preliminary analysis of the statics and kinetics of the Glarus overthrust. Eclogae Geologicae Helvetiae 62, 143–154.

Hubbert, M.K., Rubey, W.W., 1959. Role of fluid pressure in the mechanics of overthrusting faulting. Bulletin of the Geological Society of America 70, 115–166.

Hull, J., 1988. Thickness-displacement relationships for deformation zones. Journal of Structural Geology 10 (4), 431–435.

Hunziker, J.C., Frey, M., Clauer, N., Dallmeyer, R.D., Friedrichsen, H., Flehmig, W., Hochstrasser, K., Roggwiler, P., Schwander, H., 1986. The evolution of illite to muscovite: mineralogical and isotopic data from the Glarus Alps, Switzerland. Contributions to Mineralogy and Petrology 92 (2), 157–180.

Hürzeler, J.-P., Schmid, S., Abart, R., 2006. Alteration at the base of the Verrucano-hangingwall along the Glarus thrust, eastern Switzerland. In: Fourth Wiss Geosience Meeting, Bern 2006, pp. 96–97.

Jagoutz, O., 2000. Description of the Deformation Structures in the Hanging and Foot Wall of the Glarus Thrust. Ph.D. thesis, ETH Zürich, Switzerland.

Jolly, R.J.H., Sanderson, D.J., 1997. A Mohr circle construction for the opening of a pre-existing fracture. Journal of Structural Geology 19 (6), 887–892.

Kennedy, L.A., Logan, J.M., 1997. The role of veining and dissolution in the evolution of fine-grained mylonites: the McConnell thrust, Alberta. Journal of Structural Geology 19 (6), 785–797.

Kirschner, D.L., Cosca, M.A., Masson, H., Hunziker, J.C., 1996. Staircase $^{40}Ar/^{39}Ar$ spectra of fine-grained white mica: timing and duration of deformation and empirical constraints on argon diffusion. Geology 24 (8), 747–750.

Kirschner, D.L., Masson, H., Sharp, Z.D., 1999. Fluid migration through thrust faults in the Helvetic nappes (Western Swiss Alps). Contributions to Mineralogy and Petrology 136, 169–183.

Kirschner, D.L., Sharp, Z.D., Masson, H., 1995. Oxygen isotopic thermometry of quartz–calcite veins: unraveling the thermal-tectonic history of the subgreenschist facies Morcles nappe (Swiss Alps). Geological Society of America Bulletin 107 (10), 1145–1156.

Lieberman, J.E., Rice, J.M., 1986. Petrology of marble and peridotite in the Seiad ultramafic complex, northern California, USA. Journal of Metamorphic Geology 4, 179–199.

Lihou, J.C., 1996. Structure and deformational history of the Infrahelvetic flysch units, Glarus Alps, eastern Switzerland. Eclogae Geologicae Helvetiae 89 (1), 439–460.

Marquer, D., Burkhard, M., 1992. Fluid circulation, progressive deformation and mass-transfer processes in the upper crust: the example of basement-cover relationships in the external crystalline Massifs, Switzerland. Journal of Structural Geology 14 (8–9), 1047–1057.

Matthews, A., Lieberman, J., Avigad, D., Garfunkel, Z., 1999. Fluid-rock interaction and thermal evolution during thrusting of an Alpine metamorphic complex (Tinos island, Greece). Contributions to Mineralogy and Petrology 135 (2–3), 212–224.

Matthies, S., Wagner, F., 1996. On a 1/n law in texture related single orientation analysis. Physica Status Solidi B – Basic Research 196 (2), K11–K15.

Mazzucato, E., Gualtieri, A.F., 2000. Wollastonite polytypes in the $CaO–SiO_2$ system: part I. Crystallisation kinetics. Physics and Chemistry of Minerals 27 (8), 565–574.

McCaig, A.M., 1984. Fluid–rock interaction in some shear zones from the Pyrenees. Journal of Metamorphic Geology 2, 129–141.

McCaig, A.M., 1989. Fluid flow through fault zones. Nature 340, 600.

McCalpin, J.P., Nishenko, S.P., 1996. Holocene paleoseismicity, temporal clustering, and probabilities of future large ($M > 7$) earthquakes on the Wasatch fault zone, Utah. Journal of Geophysical Research 101 (B3), 6233–6254.

McConnell, J.D.C., 1995. The role of water in oxygen isotope exchange in quartz. Earth and Planetary Science Letters 136 (3–4), 97–107.

Means, W.D., 1981. The concept of steady-state foliation. Tectonophysics 78 (1–4), 179–199.

Means, W.D., 1995. Shear zones and rock history. Tectonophysics 247 (1–4), 157–160.

Mecklenburgh, J., Rutter, E.H., Burlini, L., Bystricky, M., 1999. Deformation of partially molten synthetic granite: implications for crustal rheology and granite pluton formation. AGU Fall Meeting, T51G-04.

Milnes, A.G., Pfiffner, O.A., 1977. Structural development of the Infrahelvetic Complex, eastern Switzerland. Eclogae Geologicae Helvetiae 70 (1), 83–95.

Milnes, A.G., Pfiffner, O.A., 1980. Tectonic evolution of the Central Alps in the cross section St. Gallen-Como. Eclogae Geologicae Helvetiae 73 (2), 619–633.

Molli, G., Heilbronner, R., 1999. Microstructures associated with static and dynamic recrystallization of Carrara marble (Alpi Apuane, NW Tuscany, Italy). Geologie En Mijnbouw-Netherlands Journal of Geosciences 78 (1), 119–126.

Molli, G., Conti, P., Giorgetti, G., Meccheri, M., Oesterling, N., 2000. Microfabric study on the deformational and thermal history of the Alpi Apuane marbles (Carrara marbles), Italy. Journal of Structural Geology 22 (11–12), 1809–1825.

Montési, L.G.J., Hirth, G., 2003. Grain size evolution and the rheology of ductile shear zones: from laboratory experiments to postseismic creep. Earth and Planetary Science Letters 211 (1–2), 97–110.

Nakamura, M., Yurimoto, H., Watson, E.B., 2005. Grain growth control of isotope exchange between rocks and fluids. Geology 33 (10), 829–832, doi:10.1130/G21659.

Olgaard, D.L., 1990. The role of second phase in localizing deformation. In: Knipe, R.J., Rutter, E.H. (Eds.), Deformation mechanisms, Rheology and Tectonics. Geological Society, London, Special Publications, vol. 54, pp. 175–181.

Oliver, J., 1986. Fluids expelled tectonically from orogenic belts; their role in hydrocarbon migration and other geologic phenomena. Geology 14 (2), 99–102.

Passchier, C.W., Trouw, R.A.J., 1996. Microtectonics. Springer-Verlag, Berlin Heidelberg, Germany.

Paterson, M.S., 1995. A theory for granular flow accommodated by material transfer via an intergranular fluid. Tectonophysics 245 (3–4), 135–151.

Pfiffner, O.A., 1977. Tektonische Untersuchungen im Infrahelvetikum der Ostschweiz. Mitteilungen geologisches Institut ETH und Universität Zürich N.F. 217, 1–432.

Pfiffner, O.A., 1981. Fold- and -thrust tectonics in the Helvetic Nappes (E. Switzerland). Geological Society of London, Special Publication vol. 9, 319–327.

Pfiffner, O.A., 1982. Deformation mechanisms and flow regimes in limestones from the Helvetic Zone of the Swiss Alps. Journal of Structural Geology 4 (4), 429–442.

Pfiffner, O.A., 1985. Displacements along thrust faults. Eclogae Geologicae Helvetiae 78 (2), 313–333.

Pfiffner, O.A., 1993. The structure of the Helvetic nappes and its relation to the mechanical stratigraphy. Journal of Structural Geology 15 (3–5), 511–521.

Pfiffner, O.A., Ramsay, J.G., 1982. Constraints on geological strain rates; arguments from finite strain states of naturally deformed rocks. Journal of Geophysical Research B 87 (1), 311–321.

Pieri, M., Kunze, K., Burlini, L., Stretton, I., Olgaard, D.L., Burg, J.P., Wenk, H.R., 2001. Texture development of calcite by deformation and dynamic recrystallization at 1000 K during torsion experiments of marble to large strains. Tectonophysics 330 (1–2), 119–140.

Poirier, J.P., 1980. Shear localization and shear instability in materials in the ductile field. Journal of Structural Geology 2 (1–2), 135–142.

Prior, D.J., Trimby, P.W., Weber, U.D., Dingley, D.J., 1996. Orientation contrast imaging of microstructures in rocks using forescatter detectors in the scanning electron microscope. Mineralogical Magazine 60 (6), 859–869.

Rahn, M., Mullis, J., Erdelbrock, K., Frey, M., 1994. Very low-grade metamorphism of the Taveyanne greywacke, Glarus Alps, Switzerland. Journal of Metamorphic Geology 12, 625–641.

Rahn, M., Mullis, J., Erdelbrock, K., Frey, M., 1995. Alpine metamorphism in the North Helvetic Flysch of the Glarus Alps, Switzerland. Eclogae Geologicae Helvetiae 88 (1), 157–178.

Rahn, M., Steinmann, M., Frey, M., 2002. Chloritoid composition and formation in the eastern Central Alps: a comparison between Penninic and Helvetic occurrences. Schweizerische Mineralogische und Petrographische Mitteilungen 82, 409–426.

Renner, J., Evans, B., 2002. Do calcite rocks obey the power-law creep equation? In: de Meer, S., Drury, M.R., de Bresser, J.H.P., Pennock, G.M. (Eds.), Deformation Mechanisms, Rheology and Tectonics: Current Status and Future Perspectives. Geological Society, London Special Publications, vol. 200, pp. 293–307.

Ring, U., Brandon, M.T., Ramthun, A., 2001. Solution-mass-transfer deformation adjacent to the Glarus Thrust, with implications for the tectonic evolution of the Alpine wedge in eastern Switzerland. Journal of Structural Geology 23 (10), 1491–1505.

Rutter, E.H., 1995. Experimental study of the influence of stress, temperature, and strain on the dynamic recrystallization of Carrara marble. Journal of Geophysical Research, B, Solid Earth and Planets 100 (B12), 24,651–24,664.

Rybacki, E., Paterson, M.S., Wirth, R., Dresen, G., 2003. Rheology of calcite–quartz aggregates deformed to large strain in torsion. Journal of Geophysical Research 108 (B2), doi:10.1029/2002JB001833.

Schmid, S.M., 1975. The Glarus overthrust: field evidence and mechanical model. Eclogae Geologicae Helvetiae 68 (2), 247–280.

Schmid, S.M., 1982. Laboratory experiments on rheology and deformation mechanisms in calcite rocks and their application to studies in the field. Mitteilungen geologisches Institut ETH und Universität Zürich N.F. 241, 1–106.

Schmid, S.M., Boland, J.N., Paterson, M.S., 1977. Superplastic flow in fine-grained limestone. Tectonophysics 43 (3–4), 257–291.

Schmid, S.M., Panozzo, R., Bauer, S., 1987. Simple shear experiments on calcite rocks: rheology and microfabric. Journal of Structural Geology 9 (5–6), 747–778.

Schmid, S.M., Paterson, M.S., Boland, J.N., 1980. High temperature flow and dynamic recrystallization in carrara marble. Tectonophysics 65 (3–4), 245–280.

Schmid, S.M., Pfiffner, O.A., Froitzheim, N., Schönborn, G., Kissling, E., 1996. Geophysical–geological transect and tectonic evolution of the Swiss-Italian Alps. Tectonics 15 (5), 1036–1064.

Schmocker, M., 2002. Rheology and Microfabrics of Quartz: Experimental Deformation in Torsion. Ph.D. thesis, ETH, Zürich.

Sibson, R.H., 1986. Earthquakes and rock deformation in crustal fault zones. Annual Review of Earth and Planetary Sciences 14, 149–175.

Siddans, A.W.B., 1979. Deformation, metamorphism and texture development in Permian mudstones of the Glarus Alps. Eclogae Geologicae Helvetiae 72 (3), 601–621.

Smith, C.S., 1948. Grains, phases, and interphases: an interpretation of microstructure. Transactions of the American Institute of Mining and Metallurgical Engineers 175, 15–51.

Stampfli, G.M., Borel, G.D., Marchant, R., Mosar, J., 2002. Western Alps geological constraints on western Tethyan reconstructions. Reconstruction of the evolution of the Alpine-Himalayan Orogen. In: Rosenbaum, G., Lister, G.S. (Eds.), Journal of the Virtual Explorer, 8, pp. 77–106.

Stipp, M., Stunitz, H., Heilbronner, R., Schmid, S.M., 2002. The eastern Tonale fault zone: a 'natural laboratory' for crystal plastic deformation of quartz over a temperature range from 250 to 700 °C. Journal of Structural Geology 24, 1861–1884.

Tullis, J., Snoke, A.W., Todd, V.R., 1982. Significance and petrogenesis of mylonitic rocks. Geology 10 (5), 227–230.

Twiss, R.J., 1977. Theory and applicability of a recrystallized grain size paleopiezometer. Pure and Applied Geophysics 115 (1–2), 227–244.

Urai, J.L., Means, W.D., Lister, G.S., 1986. Dynamic recrystallization of minerals. In: Hobbs, B.E., Heard, H.C. (Eds.), Mineral and Rock Deformation: Laboratory Studies. The Paterson. Geophysics Monograph, vol. 36. American Geophysical Union, Washington DC, pp. 161–199.

Van Daalen, M., Heilbronner, R., Kunze, K., 1999. Orientation analysis of localized shear deformation in quartz fibres at the brittle–ductile transition. Tectonophysics 303 (1–4), 83–107.

Van der Pluijm, B.A., 1991. Marble mylonites in the Bancroft shear zone, Ontario, Canada: microstructures and deformation mechanisms. Journal of Structural Geology 13 (10), 1125–1135.

Venables, J.A., Harland, C.J., 1973. Electron back-scattering patterns - a new technique for obtaining crystallographic information in the scanning electron microscope. Philosophical Magazine 27, 1193–1200.

White, S.H., Burrows, S.E., Carreras, J., Shaw, N.D., Humphreys, F.J., 1980. On mylonites in ductile shear zones. Journal of Structural Geology 2 (1–2), 175–187.

Wissing, S.B., Pfiffner, O.A., 2003. Numerical models for the control of inherited basin geometries on structures and emplacement of the Klippen nappe (Swiss Prealps). Journal of Structural Geology 25 (8), 1213–1227.